Material Science and Technology Division

Heavy Vehicle Propulsion Materials Program
Quarterly Progress Report for
April through June 2007

D. R. Johnson
Technical Project Manager

Prepared for
U.S. Department of Energy
Assistant Secretary for Energy Efficiency and Renewable Energy
Office of FreedomCAR and Vehicle Technologies Program
VT 05 01 020

Prepared by the
OAK RIDGE NATIONAL LABORATORY
Oak Ridge, Tennessee 37831-6066
Managed by
UT-Battelle, LLC
for the Department of Energy
Under contract DE-AC05-00OR22725

CONTENTS

Project 18518 – Materials for High Efficiency Engines

*Lightweight Valve Train Materials (*Caterpillar)

Mechanical Reliability of PZT Piezo-Stack Actuators for Fuel Injectors (ORNL)

Friction and Wear Reduction in Diesel Engine Valve Trains (ORNL)

NDE of Diesel Engine Components (Argonne)

Project 18519 – Materials for Control of Exhaust Gases and Energy Recovery Systems

Advanced Cast Austenitic Stainless Steels for High Temperature Components, CRADA with Caterpillar (ORNL)

Development of Materials Analysis Tools for Studying SCR Catalysts, CRADA with Cummins (ORNL)

Durability and Reliability of Ceramic Substrates for Diesel Particulate Filters, CRADA with Cummins (ORNL)

Catalysis by First Principles - Can Theoretical Modeling and Experiments Play a Complimentary Role in Catalysis? (ORNL)

Project 18865 – Materials by Design

Ultra-High Resolution Electron Microscopy for Characterization of Catalyst Microstructures and De-activation Mechanisms (ORNL)

Life Prediction of Diesel Engine Components (ORNL)

Powder Processing of Nanostructured Alloys Produced by Machining (Purdue)

Modeling of Thermoelectrics (ORNL)

Lightweight Valve Train Materials

Nathaniel S. L. Phillips
Caterpillar Inc.

Introduction

Valve train components in heavy-duty engines operate under high stresses and temperatures, and in severe corrosive environments. In contrast, the valve train components in the light-duty engine market require cost-effective reliable materials that are wear resistant and lightweight in order to achieve high power density. For both engine classes, better valve train materials need to be identified to meet market demand for high reliability and improved performance, while providing the consumer lower operating costs.

Advanced ceramics and emerging intermetallic materials are highly corrosion and oxidation resistant, and possess high strength and hardness at elevated temperatures. These properties are expected to allow higher engine operating temperatures, lower wear, and enhanced reliability. In addition, the lighter weight of these materials (about 1/3 of production alloys) will lead to lower reciprocating valve train mass that could improve fuel efficiency. This research and development program is an in-depth investigation of the potential for use of these materials in heavy-duty engine environments.

The overall valve train effort will provide the materials, design, manufacturing, and economic information necessary to bring these new materials and technologies to commercial realization. With this information, component designs will be optimized using computer-based lifetime prediction models, and validated in rig bench tests and short-and long-term engine tests.

Program Overview

Information presented in this report is based on previous proprietary research conducted under Cooperative Agreement DE-FC05-97OR22579.

Ceramic Materials

Silicon nitride materials have been targeted for valve train materials in automotive and diesel industries since the early 1980's. Some silicon nitride (Si_3N_4) material grades have reached a mature level of materials processing, capable of being implemented into production. Commercial realizations have been reported in both automotive and diesel valve trains, with large-scale production underway. The Si_3N_4 valve train components in production are used in high rolling contact stress applications and have exhibited superior wear resistance and longevity.

Intermetallic Materials

Titanium aluminide (TiAl) based intermetallics retain their strength at elevated temperature and are highly corrosion-resistant. They are lightweight and possess high fracture toughness. These alloys are actively being investigated for several aerospace and automotive applications.

Summary
The primary focus of this quarter was to troubleshoot problems experienced with the completion of Phase #3 engine exposure of the lightweight valves on the Caterpillar natural gas G3406 genset and to finish Phase #3. Si3N4 147-31N four point bend pins were also ordered to further study the affects of machining on the strength and durability of advanced ceramic engine components.

This quarterly report will document the will update the progress of testing on the genset engine and the machining study. Also, the plans for next quarter will be outlined.

G3406 Genset Engine Exposure – Phase #3

The problem with the charge amplifiers, as described in the 2Q FY07 Quarterly Report, were identified at Caterpillar and sent to the manufacturer for repair. The fixed amplifiers were sent back to ORNL/NTRC for reassembly on the genset upon receiving them from the manufacturer. Testing of the engine valves resumed soon after.

It was determined that the genset could run at full power (235 kW) as a result of switching the valves from in Cylinder 1 to steel valves and Cylinder 6 to new ceramic valves as outlined in previous quarterly reports. The current layout of valves is presented in Figure 1. However, late in the quarter an engine failure occurred where Cylinder 6 was not experiencing compression and the fuel injector was malfunctioning. The root cause of this failure has yet to be identified, but a failure of one of the ceramic exhaust valves in Cylinder 6 is suspected. Further investigation into this problem will be addressed early next quarter.

Si3N4 Machining Study - *HTML User Proposal No. 2003-058 "Effect of Machining Procedures on the Strength of Ceramics for Diesel Engine Exhaust Valves"*

Residual stress measurements from the SN235P Si3N4 test pins revealed a high compressive stress within the first few microns of the surface. The pins that were finish machined showed a higher compressive residual stress and a higher Weibull modulus than the pins that were rough machined, while the characteristic strength of all samples was relatively the same. This indicates that the machining of advanced ceramic components plays a larger role in the overall durability than the actual material.

A similar study will be done on 147-31N Si3N4 pins to determine what effect the machining has on the overall durability of advanced ceramic components. The pins will be exposed to a rough and finish machining process under the same machining parameters as the SN235 Si3N4 pins. However, only one parameter set of each of machining techniques will be studied to save time and expenses. It is predicted that the 147-31N Si3N4 will behave similarly to the SN235 Si3N4, further strengthening the conclusion that the durability of advanced ceramic components has more to do with the machining of the material than the material itself.

Some of the 147-31N Si3N4 pins will also be exposed to laser aided machining (LAM). LAM is better suited for the machining that would be done on the stem of the valve, instead of critical areas such as the valve head or keeper grooves. Results from the LAM tests will be studied independently from the previous machining study.

Next Steps

The completion of Phase #3 on the G3406 genset depends on results from the investigation into why Cylinder 6 was unable to complete compression. If a ceramic exhaust valve has failed as expected, then the ceramic valves will be pulled from that cylinder and replaced with production valves. The testing will then continue on the rest of Si3N4 and TiAl valves at rated conditions. Following the completion of Phase #3, the valves will be exposed to a wear analysis and a fast fracture test to determine the remaining strength of the valves after 1000 hours of engine exposure time. Surface analysis with laser scanning will also be done on the valves to detect any flaws in the surface finish following engine testing.

The 147-31N Si3N4 test pins have been received from the manufacturer and are waiting machining. After machining of the samples takes place, they will be examined with laser scattering imaging and subjected to four-point bend tests to determine Weibull Modulus and characteristic strength. Depending on the results from the four-point bend tests, residual stress measurements may also be taken from the samples. The LAM samples will undergo the same four point-bend tests as the rough and finished machined samples, but will be analyzed independently.

The study on Lightweight Valve Materials is scheduled to conclude following the next quarter. Following the completion of Phase #3, and the subsequent analysis, a final report will be written describing all of the results from the study on Si3N4 and TiAl engine valves. A final report will also be written on the results from the user proposal "*Effect of Machining Procedures on the Strength of Ceramics for Diesel Engine Exhaust Valves.*"

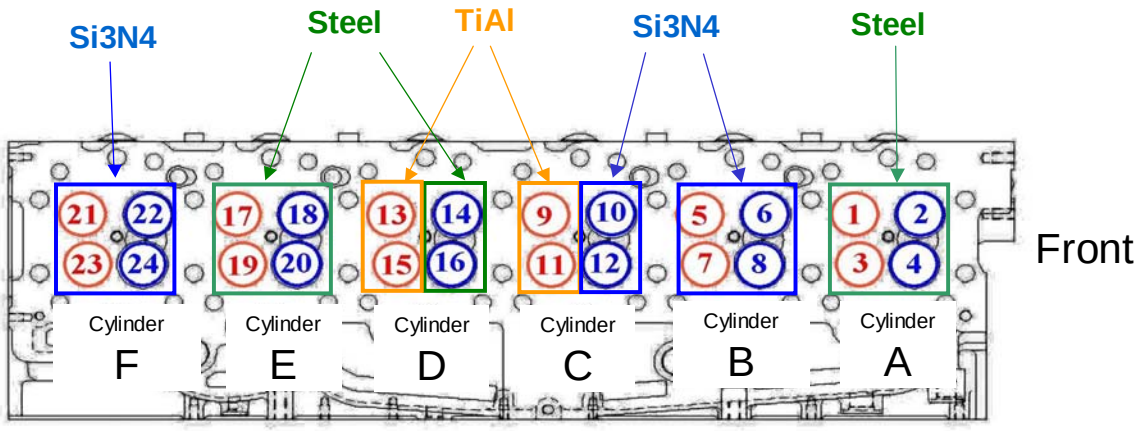

(Viewing combustion face)

Figure 1 Valve arrangement for Phase #3

Mechanical Reliability of PZT Piezo-Stack Actuators for Fuel Injectors

A. A. Wereszczak, H. Wang, and H.-T. Lin
Oak Ridge National Laboratory

Objective/Scope

The use of piezoelectric stack actuators as diesel fuel injectors has the potential to reduce injector response time, provide greater precision and control of the fuel injection event, and lessen energy consumption (e.g., for use in homogeneous charge compression ignition, HCCI, engines). Though piezoelectric function is the obvious primary function of lead zirconate titanate (PZT) ceramic stacks for fuel injectors, their mechanical reliability can be a performance and life limiter because PZT is both brittle, lacks high strength, and may exhibit fatigue (i.e., slow crack growth) susceptibility. That brittleness and relatively low strength can be overcome with proper design though. This project combines in-situ micromechanical testing, microstructural-scale finite element analysis, probabilistic design sensitivity, and structural ceramic probabilistic life prediction methods to systematically characterize and optimally design PZT piezoelectric stack actuators that will enable maximized performance and operational lifetime.

Technical Highlights

Assembly of the piezoactuator test facility was completed during the second quarter and its setup is shown in Fig. 1. The whole load train is capable of applying a static compressive load to the piezostack actuator through dead-weight loading (plans exist in FY08 to replace this with a loading actuator capable of applying a monotonically increasing force for accelerated testing). A piezostack actuator is mounted between parallel (horizontal) metal plates having two non-contact capacitance gages mounted on them. Semi-articulating (electrically insulating) silicon nitride push rods apply the static compressive force on the piezostack actuator. Even though a dead weight is used to apply a static load, a load cell is positioned in the load train to enable load measurement throughout cyclic loading. Customized software (MTIC, Oak Ridge, TN) is used to excite a high-voltage, high frequency amplifier that in turn drives the piezostack actuator. Additionally, that same software monitors applied voltage and displacement signals from the capacitance gages, and is programmable to take periodic “snapshots” of the data during high frequency testing. Voltages and displacement signals are then used to calculate electric fields, amount of charge, charge densities, and strains.

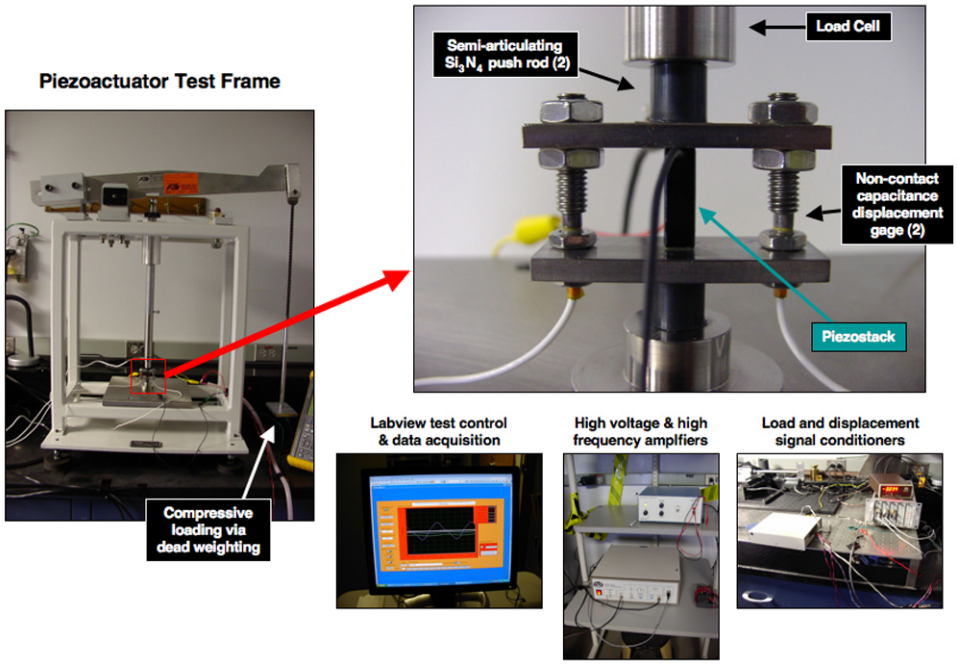

Figure 1. Piezoactuator test frame is shown at the left with an enlargement of the test assembly (with mounted piezoactuator) shown in the upper right. Subcomponents shown at lower right.

The first PZT piezostack actuator (PSI TS18-H5-104, Cambridge, MA) test involves our examining time- or cycle-dependent changes in performance over large number of cycles. This test is still ongoing as of this writing, is cycling at 10 Hz and at 150V, and has accumulated approximately 3.5 million cycles (or about 1/3 of the device's rated lifetime according to the manufacturer). As shown in Fig. 2, under a superimposed static compressive force of 150 N (6 MPa), the amount of imposed displacement and strain has reduced by ~6% over that time with that constant applied voltage.

For FY08, plans involve constructing additional test units that will have temperature control environment, an ability to monotonically increase the static load, and strategies to develop accelerated test methods. Additionally, a joint collaboration will be sought with a piezostack actuator end user.

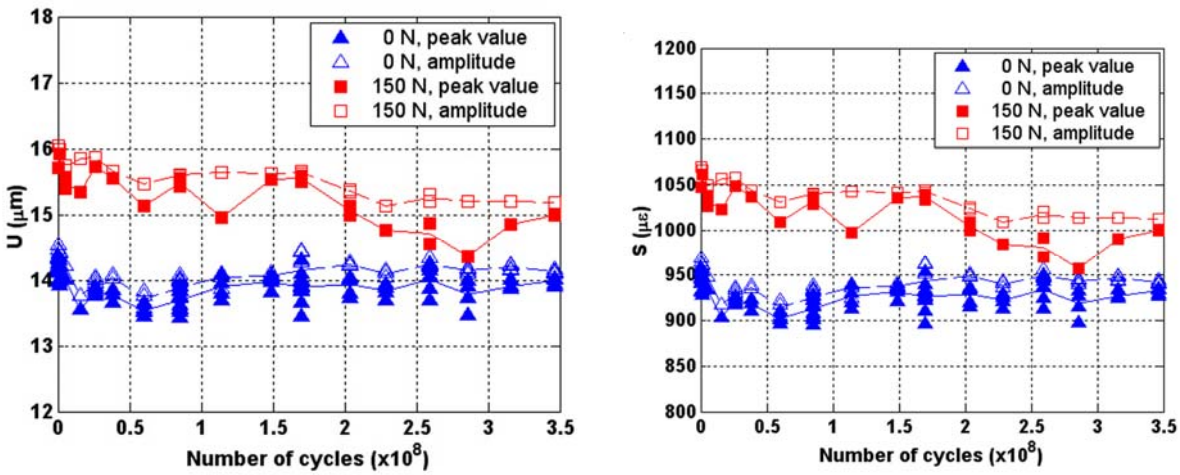

Figure 2. Changes in the amount of displacement (left) and strain (right) as a function of number of cycles.

Additional analyses continued involving the mechanical evaluation of single-layer, electroded PZT. The direction of the 1.2 kV/mm electric field affected the measured failure stress. In Fig 3. (upper left), the failure stress of the PZT was highest when the positive electrode side was the tensile side and lowest when the negative electrode size was the tensile side. The characteristic strength value for specimens in an open circuit (or no applied electric field) was between those of the other conditions. Fractography was conducted and a by-product of that was out estimation of the strength-limiting flaw size of each of the test specimens. An example of such a flaw is shown in Fig. 3 (upper right). From those flaw size measurements, we were able to estimate a critical stress intensity for each specimen, and their results are illustrated in Fig. 3 (bottom). Because strength is linkable to critical stress intensity, their ranking trends were similar; namely, the negative electrode side under an electric field was the highest as its critical stress intensity. These results clearly indicate that the applied electric field affects the failure stress and critical stress intensity of PZT.

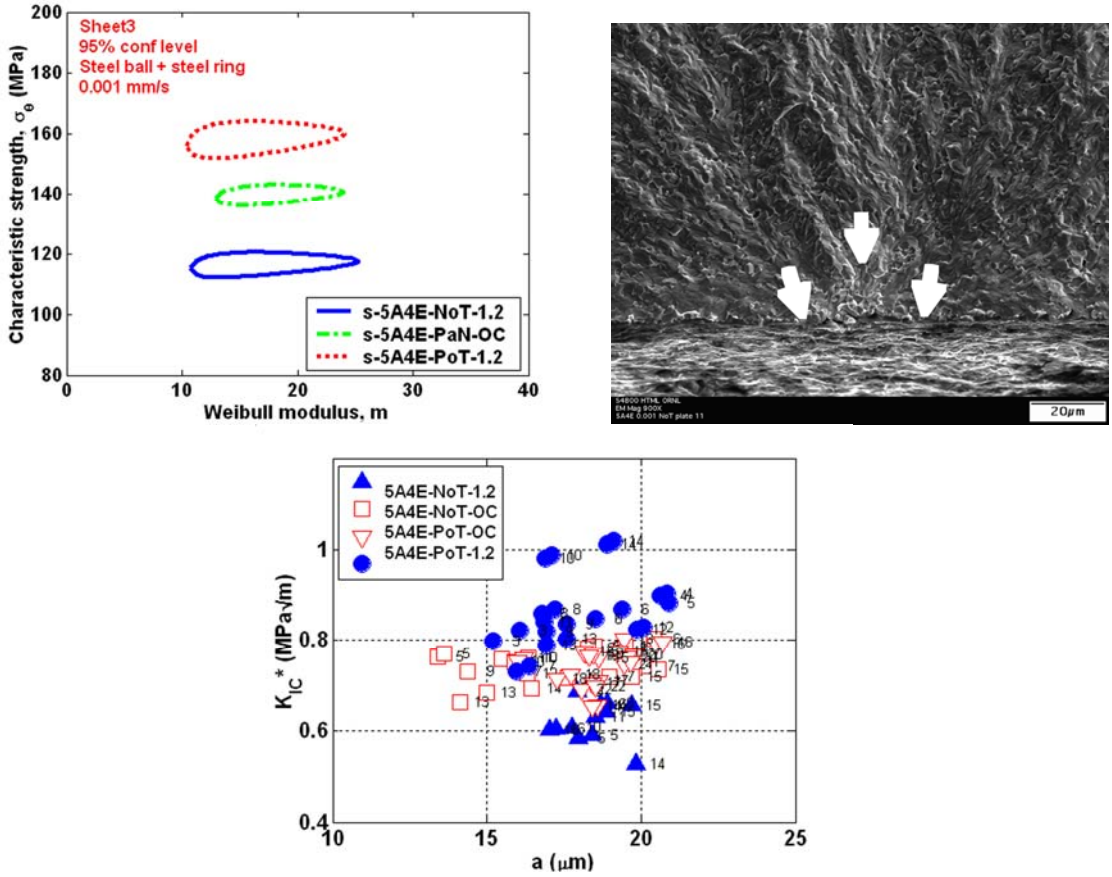

Figure 3. Upper left: 95% confidence interval of characteristic bending strength as a function of Weibull modulus for PZT with negative electrode side under tension and 1.2 kV/mm (NoT), open circuit (OC) and positive side under tension and 1.2 kV/mm (PoT). Upper right: example of strength limiting flaw. Bottom: calculated fracture toughness (K_{ic}) as a function of flaw size.

Status of FY 2007 Milestones

Establish piezoactuator reliability test facility. [09/07] *Completed.*

Communications/Visits/Travel

Wereszczak and Wang attended the Spring 2007 Meeting of the Center for Dielectric Studies at Penn State University, 9-10 April 2007.

Publications

None.

References

None.

Friction and Wear Reduction in Diesel Engine Valve Trains

Peter Blau
Oak Ridge National Laboratory

Objective/Scope

The objective of this effort is to enable the selection and use of improved materials, surface treatments, and lubricating strategies for value train components in energy-efficient diesel engines. Depending on engine design and operating conditions, between 5 and 20% of the friction losses in an internal combustion engine are attributable to the rubbing between valve train components. Wear and consequent leaks around valve seats can reduce cylinder pressure and engine efficiency. Contacting surfaces in the valve train include the valve heads, seats, tappets, guides, and stems. This effort is designed to address key rubbing interfaces within the valve train where there are opportunities to employ advanced materials and surface treatments to reduce friction and save energy.

A two-pronged, interdisciplinary approach is planned to address both materials and lubrication-related aspects. The first task concerns the design and construction of a laboratory testing apparatus to simulate the thermal, chemical, and mechanical contact environment characteristic of valves and valve seats. The second task involves improving the performance of the valve stems as they oscillate within the valve guides. Task one is under way.

Technical Highlights

Scuffing Review Completed. Scuffing is an important materials degradation and friction control issue that affects engine components like piston skirts; piston rings; fuel injector plungers; valve guides, seats, and stems; cam tappets; and more. For several years, under OFCVT sponsorship, ORNL has been systematically investigating the occurrence of scuffing under a range of engine-like conditions. That includes its initiation and propagation in alternate fuels, how to detect it by high-speed friction monitoring, how to graphically characterize its spread over time, and how to model it under boundary-lubricated systems. This work has been summarized and will be presented by P. Blau at the Engine Materials session of the Diesel Engine Efficiency and Emissions Research (DEER) Conference scheduled for August in Detroit. Based on ORNL's research and related work by others, is apparent that there are a number of possible approaches to modify the surface structure, composition, and morphology of materials to alleviate or mitigate scuffing. The problem of scuffing of both traditional and advanced materials is likely to become even more important for the next generation of bio-fueled diesel engines. Those issues will also be discussed in the DEER presentation.

Ionic Liquids. Another important issue related to the reduction of scuffing is the development of improved lubricants. Ionic liquids are clean, stable, low vapor pressure alternatives to traditional engine lubricants. Recently, the ORNL management team provided internal funds to explore the potential of these synthetic fluids. Jun Qu, who led the research team, will present a paper on these results in the Fuels and Lubricants

the DEER Conference. The possibility of using ionic liquids as non-catalyst poisoning additives to mineral oil makes them attractive candidates for new, cleaner oils with viscosities that are adjustable by molecular engineering. Patents have been filed in this area.

Repair of the Scanning Acoustic Microscope. For nearly half a year, ORNL's Scanning Acoustic Microscope (SAcM) has been out of service, and that has hampered our ability to study subsurface damage on test specimens, machined surfaces, and coatings. The instrument, which also supports projects in the High Temperature Materials Laboratory User Program, uses high-frequency sound waves (100 kHz – 2 GHz) to create images of cracks, flaws, voids, coating interfaces, and surface treatments in a zone several micrometers deep within metal and ceramic surfaces. These images can be used to determine the subsurface feature sizes and orientations, and can indicate residual stress patterns as well. At last, repairs on a critical electronics component have been completed in Germany, and it is expected that the SAcM will be back in operation within the next month.

Future Plans

1) Complete repairs of the scanning acoustic microscope.

2) Present two talks at the DOE Diesel Engine Efficiency and Emissions Research (DEER) Conference in Detroit in August. One will be on the origins, measurement, and control of scuffing in diesel engine components and the second will discuss ionic liquids.

Travel

None

Status of Milestones

1) Complete first matrix of tests to compare traditional and advanced valve/valve seat materials at high temperature, in controlled-atmosphere, and with repetitive impact conditions. Submit report or journal article on the results. **(03/07) –** *delayed due to unanticipated changes in FY 2007 funding.*

2) Prepare an analysis of the basic mechanisms that operate as valve/valve seat materials degrade in service and correlate them with basic material properties and metallurgical structure. Submit report or journal article describing the analysis. – *delayed due to unanticipated changes in FY 2007 funding* **(09/07)**

Publications and Presentations

None

NDE of Diesel Engine Components

J. G. Sun and N. Phillips*

Argonne National Laboratory
***Caterpillar, Inc.**

Objective/Scope

Emission reduction in diesel engines designated to burn fuels from several sources has lead to the need to assess ceramic valves to reduce corrosion and emission. The objective of this work is to evaluate several nondestructive evaluation (NDE) methods to detect defect/damage in structural ceramic valves for diesel engines. One primary NDE method to be addressed is elastic optical scattering. The end target is to demonstrate that NDE data can be correlated to material damage as well as used to predict material microstructural and mechanical properties. There are two tasks to be carried out: (1) Characterize subsurface defects and machining damage in flexure-bar specimens of NT551 and SN235 silicon nitrides (Si_3N_4) to be used as valve materials. Laser-scattering studies will be conducted at various wavelengths using a He-Ne laser and a tunable-wavelength solid-state laser to optimize detection sensitivity. NDE studies will be coupled with examination of surface/subsurface microstructure and fracture surface to determine defect/damage depth and fracture origin. NDE data will also be correlated with mechanical properties. (2) Assess and evaluate surface and subsurface damage in Si_3N_4 and TiAl valves to be tested in a bench rig and in an engine. All valves will be examined at ANL prior to test, during periodic scheduled shut downs, and at the end of the planned test runs.

Technical Highlights

Work during this period (April-June 2007) focused on developing the cross-polarization confocal microscopy system and evaluating an optical coherence tomography (OCT) system for high-resolution 3D imaging of the subsurface of silicon-nitride ceramics.

1. Laser-Scatter NDE Evaluation of Engine-Tested Valves

Mr. Nate Phillips of Caterpillar Inc. has informed ANL the failure of ceramic valves running in the natural gas G3406 generator set at NTRC. An intake valve failed after 55 hours at full load, causing the rest of the valves in that cylinder to be destroyed. The ceramic pieces were also sucked into the other cylinders, damaging all other ceramic and TiAl valves so they cannot be used further. As a result, the natural gas engine test will be ending and analyses will be conducted to these 500-h engine-tested valves. It was planned that Dr. H.-T. Lin of ORNL will perform failure analysis and ANL will perform NDE analysis. At this time, the initial failure was suspected to be at the keeper notch region, which will be verified from the failure analysis, ANL will therefore first examine the previous NDE data for that valve (valve number is unknown at present) and determine the flaw type that could have caused the failure. It was noted that severe machining damage in the keeper notch edges from the original “coarse” machining of these ceramic valves had caused a premature failure of a ceramic valve in the bench test (see quarterly reports for the period of April-June 2004 by Grassi et al. of Caterpillar and by ANL).

2. Development of a Cross-Polarization Confocal System for Measurement of 3D Subsurface Microstructure in Silicon Nitride Ceramics

In the quarterly report for the previous period, we have identified two issues for the confocal system when applied for imaging silicon nitrides: (1) poor accuracy in lateral scan direction and (2) shallow detection depth. Effort in this period was directed to address the first problem. We have evaluated a newly purchased scan stage that has a specified accuracy of 0.2 µm. We found that the stage cannot maintain a constant speed which is critical for linear-scan accuracy. However, by modifying the data acquisition program and using a lower speed, the current scan stage was able to produce reasonable results. Figure 1 shows a comparison of two cross-sectional scan images of a micro-ruler with the marks spaced at 10 µm apart. The alignment of the marks in the lateral direction is much better after the modification (Fig. 1b) than before (Fig. 1a). The alignment error between the scan lines (50 lines in each image) is now typically <1 µm. For the second issue, we have ordered a wavelength division multiplexer which allows for the confocal system to be operated at a visible or an infrared wavelength. Work to implement this device will be reported in next period.

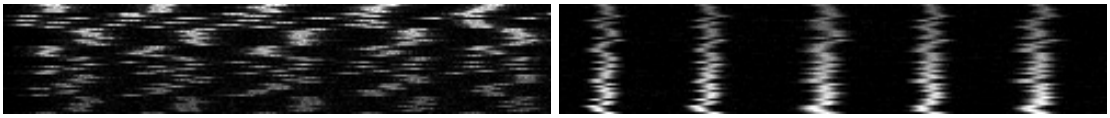

(a) (b)

Fig. 1. Scan images of a micro-ruler surface at (a) before and (b) after data-acquisition program modification. Size of images is 50 µm x 5 µm.

3. Optical Coherence Tomography (OCT) for 3D Imaging of Ceramic Subsurface

OCT is a 3D method originally developed for imaging biological materials. It utilizes a Michelson interferometer to differentiate optical reflection from different depths of a translucent material. The block diagram of the OCT system at ANL is shown in Fig. 2. Light from an optical source is split into two paths, a sample path and a reference path. Light in the reference path is reflected from a fixed-plane mirror, whereas light in the sample path is reflected from surface and subsurface features of a ceramic sample. The reflected light from the sample path will only be detected if it travels a distance that closely matches the distance traveled by the light in the reference path. Thus, by scanning the sample, data can be obtained in a plane perpendicular or parallel to the sample surface. For an OCT system, typically spatial resolutions are in the range of 5–15 µm when a low-coherence diode laser is used.

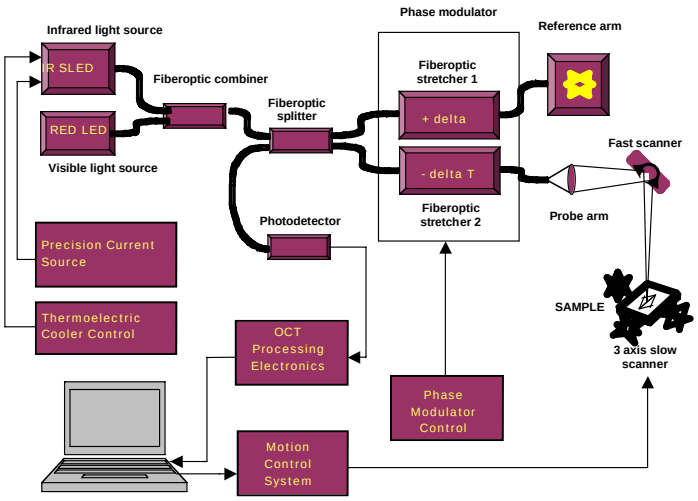

Fig. 2. Block diagram of basic elements in OCT system.

Although OCT has lower resolution than the confocal method, OCT systems typically use optical sources of longer wavelengths (the ANL system uses a 1310 nm diode laser) that are capable for deeper optical penetration for ceramics than visible wavelengths typically used by confocal systems. The ANL OCT was evaluated to scan the cross sections of a NT551 and a SN235P step wedge. Figure 3 shows the micrographs of the step-wedge edges with listed average thickness for each step. The corresponding OCT scan images are shown in Fig. 4. For the NT551 step wedge, the top and bottom surfaces of the first three steps (34, 84, and 184 µm thick) are visible, while those for the first two steps (35 and 84 µm thick) are detected (a third line below the wedges comes from a mirror surface which supported the wedges during the scan). The optical thickness of the wedge steps can be directly determined from the images. Because optical penetration depth for OCT equals the physical depth multiplied by the refraction index of the material, direct comparison of optical and physical depths allows for the determination of the refraction index of silicon nitrides, which are not well documented (some conflicting data exist in the literature). The measured refection index for both NT551 and SN235P is 2.0, which is consistent with reported values for deposited silicon-nitride films. In addition, the OCT images in Fig. 4 reveal many scattering sources within the NT551 and SN235P subsurface. Higher scattering is usually an indication of porosity or defects; this method may therefore be used for NDE of these ceramics. This capability will be further investigated in the next period.

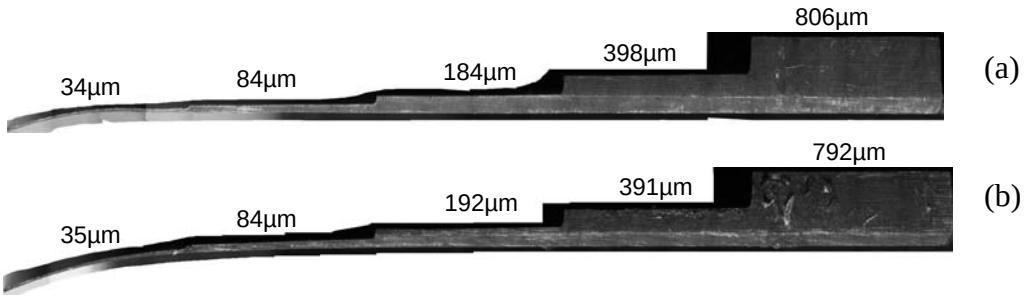

Fig. 3. Micrographs and average thickness at edges of (a) NT551 (b) SN235P step wedges.

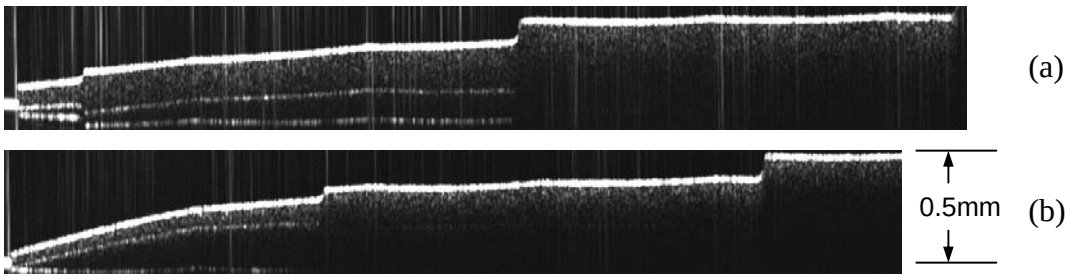

Fig. 4. Scanned cross-sectional OCT images for (a) NT551 and (b) SN235P step wedges.

Status of Milestones

Current ANL milestones are on schedule.

Communications/Visits/Travel

None this period.

Problems Encountered

The laser used for the confocal system was not working, and it was returned to the manufacturer for evaluation and repair. The problem is expected to be fixed in July 2007.

Publications

An invited manuscript entitled "Evaluation of Silicon-Nitride Ceramic Valves," coauthored by J. G. Sun, J. M. Zhang, J. S. Trethewey, N. S. L Phillips, and J. A. Jensen, was submitted to the International Journal of Applied Ceramic Technology in April 2007.

An abstract entitled "Effect of Machining Procedures on the Strength of Ceramics for Diesel Engine Valves," coauthored by N. S. L. Phillips, J. A. Jensen, M. J. Andrews, J. S. Tretheway, D. M. Longanbach, H. T. Lin, and J. G. Sun, has been submitted to the Diesel Engine-Efficiency and Emissions Research (DEER) 2007 Conference.

Advanced Cast Austenitic Stainless Steels for High Temperature Components

P. J. Maziasz, John P. Shingledecker, and N. D. Evans
Oak Ridge National Laboratory

M. J. Pollard,
Caterpillar, Inc.

Objective/Scope

This is the 2nd ORNL CRADA project with Caterpillar. This CRADA project is focused on commercialization of the new CF8C-Plus cast austenitic stainless steel, which was developed during the first ORNL/CAT CRADA. CF8C-Plus stainless steel is a cost-effective material upgrade for much more performance, durability and temperature capability relative to current heavy-duty diesel engine exhaust components made from SiMo ductile cast iron. In FY2005, this project completed the initial properties data base needed for alternate materials selection, and component design or redesign, including fatigue, thermal fatigue, and creep, and studies of aged materials. In FY2006, longer term creep-testing and fatigue studies at much lower frequencies were completed, together with new tests directly related to specific new component applications, like turbocharger housings. This CRADA (Cooperative Research and Development Agreement) project (ORNL02-0658) was extended beyond the initial 3-year term last year, and another 12 month extension was initiated this quarter, so that this project will now end in July, 2008. Requests for more detailed information on this project should be directed to Caterpillar, Inc.

Highlights

Caterpillar, Inc.

The Caterpillar Regeneration System (CRS) components cast from CF8C-Plus steel went into production at the beginning of 2007, and are currently on all heavy-duty highway truck diesels since the beginning of 2007. Trial licenses for several new commercial applications were signed by Caterpillar this quarter. Caterpillar and ORNL worked together to present the ballot for an ASTM new alloy designation for CF8C-Plus stainless steel in May, 2007.

ORNL

Stainless Foundry & Engineering (SF&E, one of the three current trial-licensees) completed successful testing of CF8C-Plus welds for the ASTM Weld Procedure Qualification last quarter. Welding behavior was good, showing the U-bend and tensile ductility required. SF&E (Ron Bird) prepared and presented a data package for approval of a new alloy grade (HG10MNN) for the ASTM A297 Specification to the Committee in May, 2007. ORNL and CAT began a 12 month extension of the CRADA project with a new end date in July, 2008, to enable the

needed testing and evaluation of thin-section casting relevant to diesel turbocharger housings.

Technical Progress, 3rd Quarter, FY2007

Background

Current cast iron heavy diesel engine exhaust manifolds and turbocharger housings are being pushed beyond their temperature capabilities as normal duty cycles approach or exceed 750°C; the rapid and severe thermal cycling contributes to increased failures. The new cast CF8C-Plus austenitic stainless steel has now been commercialized, and business opportunities for exclusive licensing are being pursued and supported for this and other high-temperature applications. Caterpillar, Inc. and ORNL have completed the systematic and thorough initial properties data base required by designers to optimize component design. Currently, more detailed and component-specific testing is in progress and needed to support trials or prototyping for new CF8C-Plus stainless steel turbocharger housings and other diesel exhaust component commercial scale-up applications.

Approach

Multiple commercial heats of CF8C-Plus stainless steel have been cast by several commercial foundries, including static sand and centrifugal casting methods. Now, both large and small prototype CF8C-Plus components have been cast. In July 2004, a large turbine housing for an industrial gas-turbine was cast by MetalTek, International, Inc. from an 8000 lb heat of the new CF8C-Plus stainless steel. In 2005, three foundries obtained trial-licenses for CF8C-Plus steel, including MetalTek and Stainless Foundry & Engineering. By the end of 2005, over 31,000 lb of CF8C-Plus components have been cast, including exhaust manifolds, and some new, thin-walled piping. In 2005, new commercial heats of CF8C-Plus Cu/W were made. In 2006, the new CF8C-Plus Cu/W was found to have more tensile strength and more creep resistance than CF8C-Plus at 750°C and above. In January 2007, Caterpillar began full-scale production of CF8C-Plus for the Caterpillar Regeneration System (CRS) burner housing. CRS exhaust components are now included on all highway heavy-duty truck diesel engines. Testing and evaluation to support and enable the use of CF8C-Plus steel for turbocharger housings is now in-progress.

Technical Progress – Caterpillar, Inc.

After completing the initial prototyping and qualification testing, Caterpillar began using the new cast CF8C-Plus stainless steel for the housing of the Caterpillar Regeneration System (CRS) for on-highway truck diesel engines at the beginning of 2007. The CRS device burns diesel fuel in the exhaust stream to heat the diesel particulate filter, in order to oxidize soot and regenerate the filter. This component is subject to extreme temperatures and thermal cycling, which makes the CF8C-Plus stainless steel a durable and relatively low-cost choice for this application.

This quarter, Caterpillar licensed CF8C-Plus cast stainless steel for trials and testing for several different end-user applications, including turbocharger housings.

Technical Progress – ORNL

Stainless Foundry & Engineering (SF&E, is one of the three current steel foundry trial-licensees) completed casting, welding and testing of plates of CF8C-Plus steel for the ASTM Weld Procedure Qualification. CF8C-Plus was found to be weldable, consistent with several prior weld-trials, and had more than enough ductility required to pass the tensile and U-bend ductility requirements for ASTM Weld Procedure Qualification. Comparison of the new CF8C-Plus Cu/W showed that it also had similar good weldability and metal fluidity relative to the standard CF8C-Plus steel. SF&E (Ron Bird) prepared the final package for approval of the new alloy grade (HG10MNN) for the ASTM A297 Specification, including tensile data on more than 10 commercial heats of CF8C-Plus cast austenitic stainless steel.

SF&E previously made step castings of both CF8C-Plus and –Plus Cu/W to evaluate the properties of thin-section casting that are directly relevant to turbocharger housing components. 24 step-cast ingots were received at ORNL for further evaluation, 12 of the standard CF8C-Plus steel and 12 of the new CF8C-Plus Cu/W steel. The initial data shows significant refinement of the dendrite/grain structure in the 0.25 inch thick step relative to the 1.0 inch thick step. The thin sections show more tensile strength at room temperature and similar strength at 700 and 800°C relative to thicker sections. Creep rupture testing of specimens from thin-sections began this quarter and will continue next quarter.

Communications/Visits/Travel

Detailed team communications between ORNL and Caterpillar occur regularly. The new 3 year CRADA began on July 21, 2002, when the previous CRADA ended and is scheduled to end on July 21, 2005. The two-year ORNL/Caterpillar CRADA extension was done last year until July 21, 2007, but this quarter, ORNL and CAT applied for another 12 month extension until July, 2008, to support the new licensing applications for CF8C-Plus steel, including diesel turbocharger housings.

Status of Milestones

Test properties of prototype components made of CF8C-Plus or –Plus Cu/W in support of diesel exhaust components, or other parts made by trial-licensee foundries for commercial applications (May 2007). Completed, because step castings are relevant to both CRS and to new turbocharger housing applications.

Publications/Presentations/Awards

Patents:
U.S. Patent 7,153,373 B2 on “Heat and Corrosion Resistant Cast CF8C Stainless Steel With Improved High Temperature Strength and Ductility,” by P. J. Maziasz, T. McGreevy, M. J. Pollard, C. W. Siebenaler, and R. W. Swindeman, was obtained on December 26, 2006.

U.S. Patent Application 11/495,671 on “Heat and Corrosion Resistant Cast Austenitic Stainless Steel Alloy with Improved High Temperature Strength,” by P. J. Maziasz, M. J. Pollard, and J. P. Shingledecker was filed on July 31, 2006.

Publications:
A draft paper “Developing New Cast Austenitic Stainless Steels with Improved High-Temperature Creep-Resistance” by P. J. Maziasz, J. P. Shingledecker, N. D. Evans and M. J. Pollard (PVP2007-26840) was peer-reviewed and accepted for publication in the Proceedings of CREEP8 – The Eighth International Conference on Creep and Fatigue at High Temperatures, to be held July 22-26, 2007 in San Antonio, TX.

Presentations:
An invited talk, “Designing New Steels for High-Temperature Service,” was presented by P.J. Maziasz at the American Metals Market (AMM) Conference on Stainless and Its Alloys, Panel IV: Technological – Metallurgical Advances, on April 10, 2007 in Pittsburgh, PA.

Development of Materials Analysis Tools for Studying SCR Catalysts

Thomas Watkins, Larry Allard, Michael Lance, Harry Meyer and Larry Walker
Oak Ridge National Laboratory

Zheng Liu, Cheryl Klepser and Tom Yonushonis
Cummins Inc.

Objective

The purpose of this effort is to produce a quantitative understanding of the process/product interdependence leading to catalyst systems with improved final product quality, resulting in diesel emission levels that meet the 2010 emission requirements.

Samples and Approach

A Cummins catalyst supplier provided new commercial Fe-zeolite powder, both fresh and degreened, which are being examined with diagnostic tools developed under the CRADA. Here, degreened means the powder was heated to 500, 700, 900 and 1100°C for 12 hours in air. Investigations of these candidate-production materials are being implemented on both the bench and engine research scale. These investigations include the examination of unused, reactor and engine-aged catalyst samples. Investigative tools included transmission electron microscopy (TEM), X-ray diffraction (XRD), X-ray photoelectron spectroscopy (XPS), Raman Spectroscopy and infrared spectroscopy (IR).

Technical Highlight

Phase identification of the fresh, commercial Fe-zeolite powder by XRD proved difficult given the vast number of zeolite structures. However, examination of the literature revealed that this powder is a beta zeolite[i] (see Figure 1). Newsham et al. examined a similar material with both XRD and TEM and simulated a XRD patterns which indicated that this material is a combination of a ~40% tetragonal and ~60% monoclinic polymorphs. Further, high stacking fault densities result in the observed sharp and broad peaks. The fresh Fe-zeolite XRD pattern looks very similar to that from a Co-(beta) zeolite[ii] suggesting that the specific catalytically active cation has little influence on the overall XRD pattern. The fresh Fe-zeolite powder was degreened at 500, 700, 900 and 1100°C for 12 hours in air, cooled to room temperature and scanned. In Figure 2, the XRD patterns show little change until 900°C, where a change in relative peak intensities and shape for the reflections at ~21.5 and 22.5 °2θ is evident. The phase composition of the powder has changed after the 1100°C exposure wherein Fe_2O_3 and Crystobalite (SiO_2) are forming (see Figure 3). Further work on Fe/zeolite fresh and aged powders will be carried out in the coming quarter.

Raman spectra were collected on the fresh and degreened samples using an Ar^+ ion laser operating at 5145 Å. This wavelength is not ideal for these samples, producing large background fluorescence signal from the fresh sample which swamped the Raman peaks. Typically, an ultraviolet (UV) laser to characterize these materials is

used.[iii] Nevertheless, following heating, the fluorescence dropped dramatically, and Raman spectra was successfully obtained. In Figure 4, the spectra acquired from the samples degreened at 500°C and 1100°C show peaks characteristic of silicate structure such as the Si-O stretching vibration at peak at ~1100 cm^{-1} and Si-O-Si bending around 500 cm^{-1}. Strong –OH vibrations are observed around 3500 cm^{-1}. Following heating at 1100°C, a peak is observed at 1500 cm^{-1} which may be associated with the formation of a metal oxide or a phase change in the zeolite. Further work will be performed on zeolite samples in the next quarter. Also, a new UV-Raman system has been purchased by another group at ORNL which will be accessible for this program and is expected to greatly improve the spectra by eliminating the background fluorescence.

Meetings

Thomas Watkins, Larry Allard, Michael Lance and Ray Johnson traveled to CTC and met with Cummins personnel on June 27.

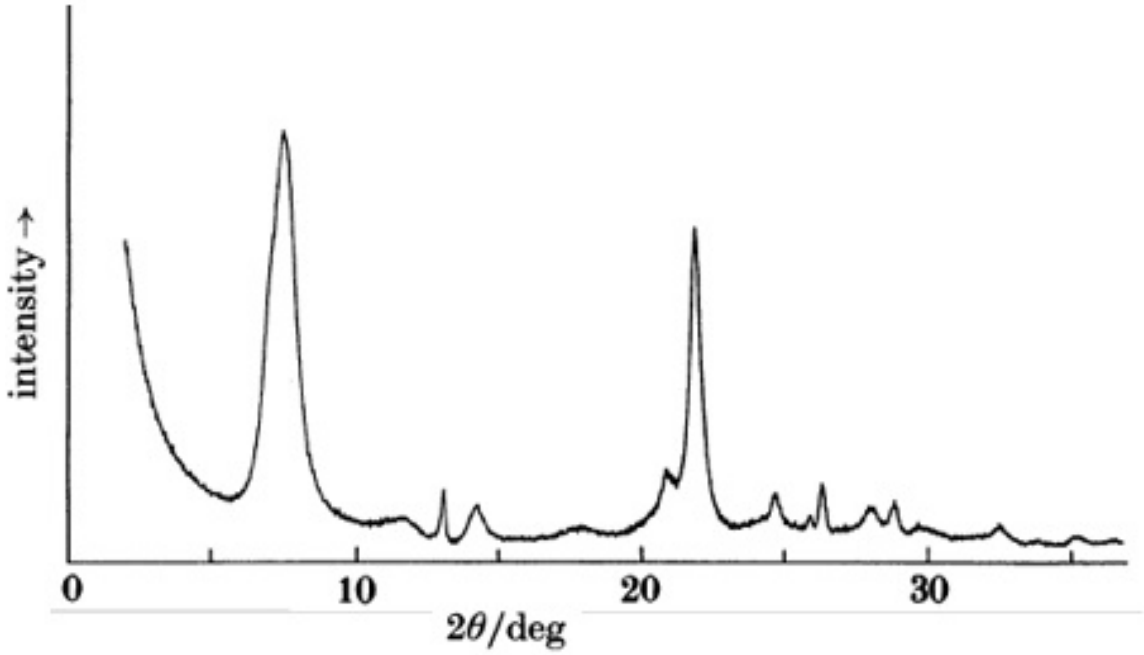

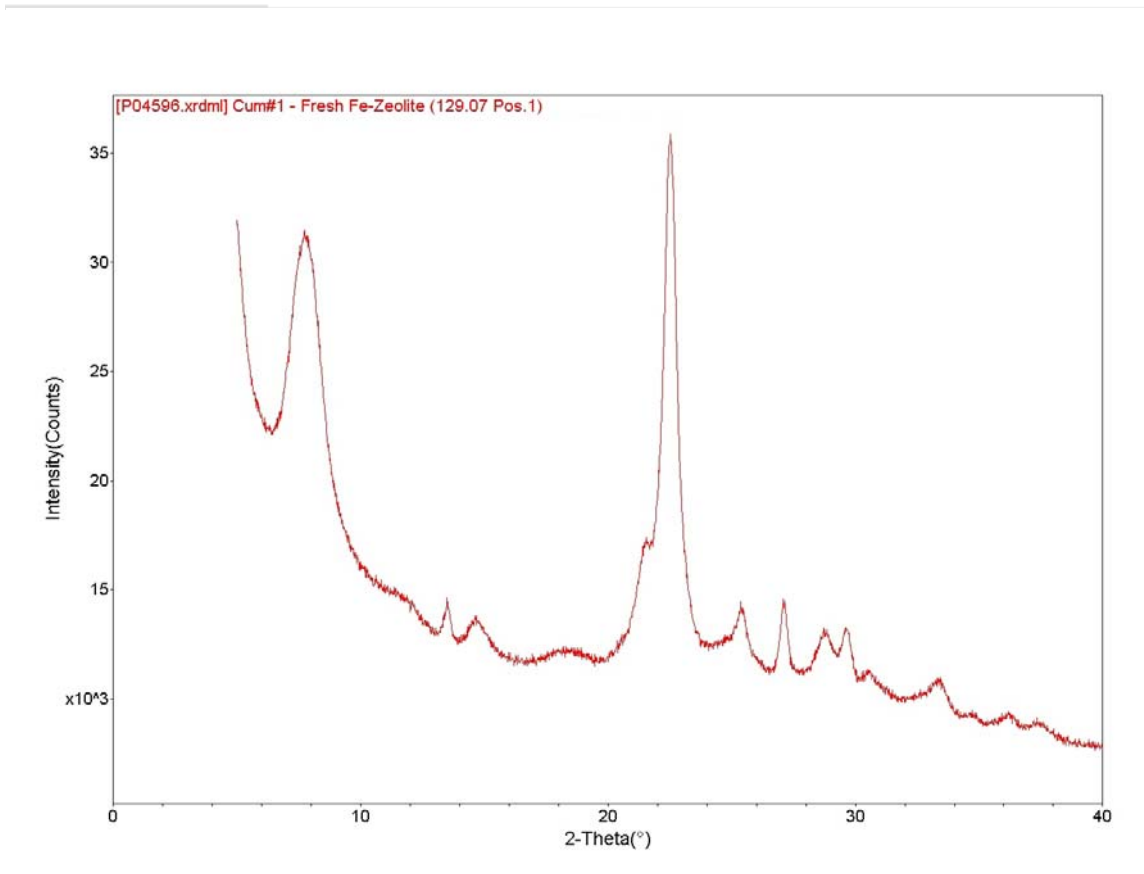

Figure 1. Comparison of the x-ray patterns for the fresh Fe-zeolite powders and those from Newsham et al.

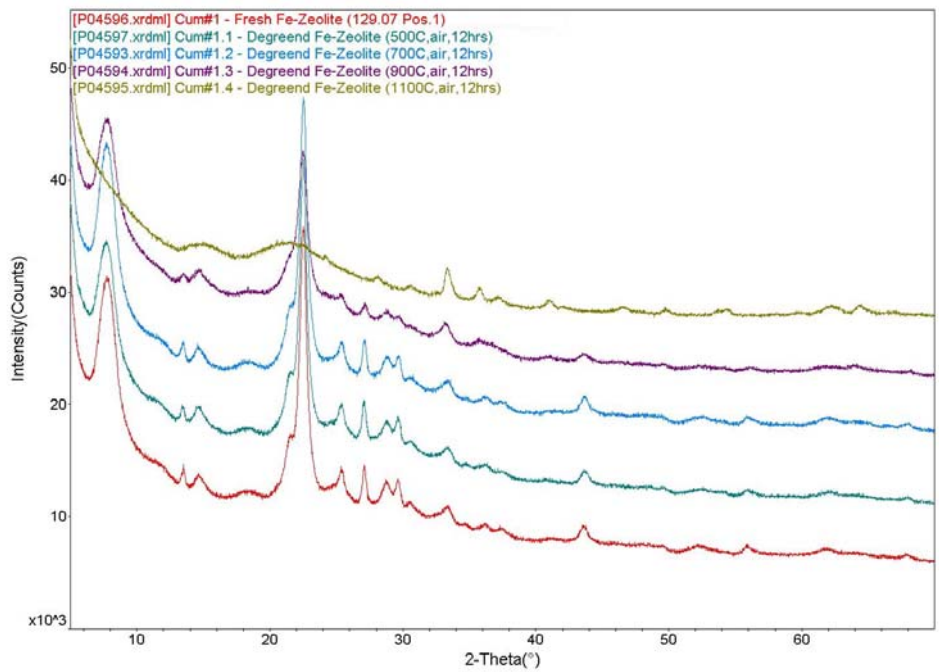

Figure 2. The x-ray patterns for the as-received and degreened Fe-zeolite powders.

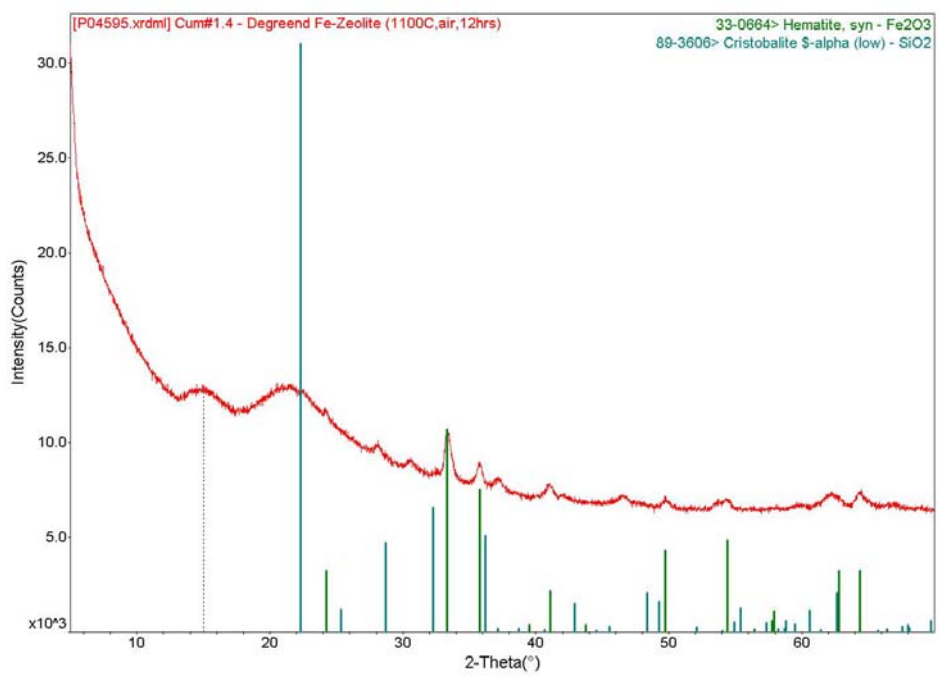

Figure 3. The x-ray pattern for the degreened Fe-zeolite powder (1100°C in air for 12 hrs). The peak at 15°2θ is unidentified.

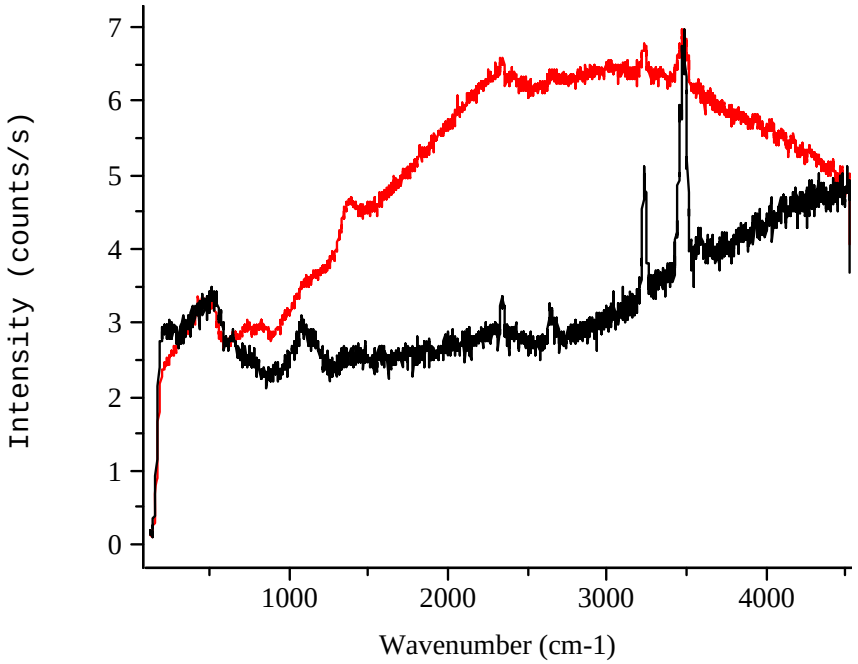

Figure 4. Raman spectra from the degreened sample at 500°C (black) and 1100°C (red).

References

[i] J. M. Newsham, M. M. J. Treacy, W. T. Koetsier, C. B. De Gruyter, "Structural Characterization of Zeolite Beta," Proc. Royal Soc. London, A. Math & Phys. Sci. **420** [1859] 375-405 (1988).

[ii] H. H. Chen, S.-C Shen, X. Chen, S. Kawi, "Selective Catalytic Reduction of NO over Co/beta-seolite: effects of synthesis conditions of beta-zeolites, Co precursor, CO loading method and reductant," *App. Cat. B* **50** 37-47 (2004).

[iii] C. Li, "Identifying the isolated transition metal ions/oxides in molecular sieves and on oxide supports by UV resonance Raman spectroscopy," *J. Catal.* **216** [1-2] 203-212 (2003).

Durability and Reliability of Ceramic Substrates for Diesel Particulate Filters

Amit Shyam and Thomas R. Watkins
Oak Ridge National Laboratory

Tom Yonushonis and Randy Stafford
Cummins Inc.

Objectives/Scope

To develop/implement test methods to characterize the physical and mechanical properties of ceramic diesel particulate filters (DPFs), and to implement a probabilistic-based analysis to quantify their durability and reliability.

Highlights

- The mechanical and thermal expansion properties of several candidate diesel particulate substrates were evaluated.
- The thermal shock resistance of the substrates was estimated based on the evaluated properties.

Technical Progress

Procedures for evaluating the mechanical properties (fracture toughness by double-torsion and elastic modulus by resonant ultrasound spectroscopy-RUS) of DPF substrates have been developed and reported earlier. In this reporting period, the comparative mechanical properties and relative thermal shock resistance of several DPF substrates was assessed. The cordierite substrates analyzed are designated C-0 and C-1, corresponding to manufacturer C in the uncoated and coated conditions, respectively and B-0, B-1 and B-2 corresponding to manufacturer B in the uncoated, coated and coated+aged conditions, respectively. In addition, a mullite DPF substrate, D-1, was analyzed in comparison to the cordieritic substrates. Since the original wall thickness of the C-0 filters was around 1.5X the other substrates, some thinner C-0 specimens were fabricated for fracture toughness comparison. The mean thickness of the C-0 specimens for double-torsion testing and resonant ultrasound spectroscopy was 0.375 mm, whereas the mean thickness of all the other specimens (including thin specimens of C-0) was 0.275 mm.

The room temperature fracture toughness of the substrates (see Figure 1) was calculated based on the double-torsion methodology. Here, the mullite substrate (D-1) has a higher fracture toughness of 0.67 $\pm$0.13 MPa$\sqrt{m}$ compared to the cordierite based substrates whose mean fracture toughness varies between 0.18-0.38 MPa$\sqrt{m}$. This is due to the interlocking “needle-like” structure of the mullite DPF substrate shown in Figure 2. For the cordierite substrates, there was little influence of coating on the room temperature fracture toughness for both manufacturers B and C. This can be inferred by comparing B-0 to B-1 and C-0 thin to C-1 in Figure 2. The fracture toughness of the thin C-0 specimens was marginally lower compared to C-0 specimens with a mean thickness of 0.375 mm. The average fracture toughness of the substrates from

manufacturer C was, however, nearly twice the toughness of the substrates from manufacturer B. The variation in the toughness of the cordierite substrates can be explained based on results in Figure 3. For all substrates, the fracture toughness increases with increasing density or alternatively the toughness decreases with increasing porosity. The density was calculated based on a mass per unit volume calculation, and the porosity of the substrates was calculated assuming a bulk density value for cordierite of 2.46 g/cc. The fracture toughness is highly sensitive to porosity, and a 20% increase in porosity causes a 50% decrease in fracture toughness.

The room temperature elastic modulus of the substrates was calculated based on resonant ultrasound spectroscopy (RUS, see Figure 4). Isotropic elasticity was assumed for RUS analysis. The mullite substrate with an elastic modulus of 25.6 GPa is stiffer than the cordierite substrates, where the modulus values range from 9.4–11.9 GPa. The other trends observed for fracture toughness of cordierite substrates are also observed for elastic modulus, namely (i) there is little influence of coating on the modulus of the substrate at room temperature, (ii) the modulus of the substrate from manufacturer C is higher than the modulus of the substrate from manufacturer B and (iii) there is a correlation between the modulus and porosity/density of the substrate.

The thermal expansion behavior of the substrates was analyzed on cellular structures in directions that were parallel and perpendicular to the extrusion direction. The average coefficient of thermal expansion (CTE) between 20 and 1000°C (see Figure 5) of the mullite substrate was much higher than those of the cordierite substrates. In addition, the CTE values for the cordierite substrates are higher in the direction perpendicular to the extrusion direction.

A simple thermal shock resistance parameter, R_S, was calculated based on the ratio of the strength of the material and the product of modulus (E) and CTE (α), i.e. $R_S = (\sigma/\alpha E)$. A modified parameter called R_K is proposed herewith, where $R_K = (K_{IC}/\alpha E)$. The value of the R_K parameter was calculated for all the substrates and has been compared in Figure 6. The values used for the calculation are room temperature elastic modulus and fracture toughness and average CTE values between 20 and 1000°C. In Figure 6, C-1 material will have the highest thermal shock resistance, whereas D-1 would have the lowest resistance. It is to be cautioned that the values of the R_K parameter can change drastically for a different temperature range so the comparison in Figure 6 is only for illustrative purposes. Moreover, a real filter has heterogeneities that a calculation like the one presented above cannot account for.

Meetings

Watkins and Shyam traveled to CTC and met with Cummins personnel on June 27.

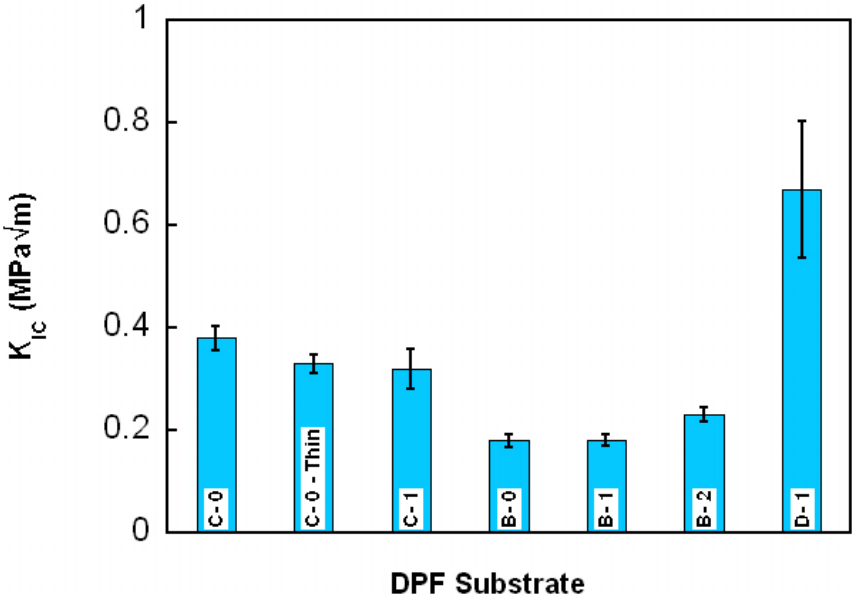

Figure 1. The room temperature fracture toughness of the DPF substrates analyzed. The mullite substrate (D-1) has a higher fracture toughness compared to the cordierite based substrates. Five specimens each were tested for C-0, C-0-Thin, C-1, B-0, B-1. Three specimens were tested for B-2 and D-1.

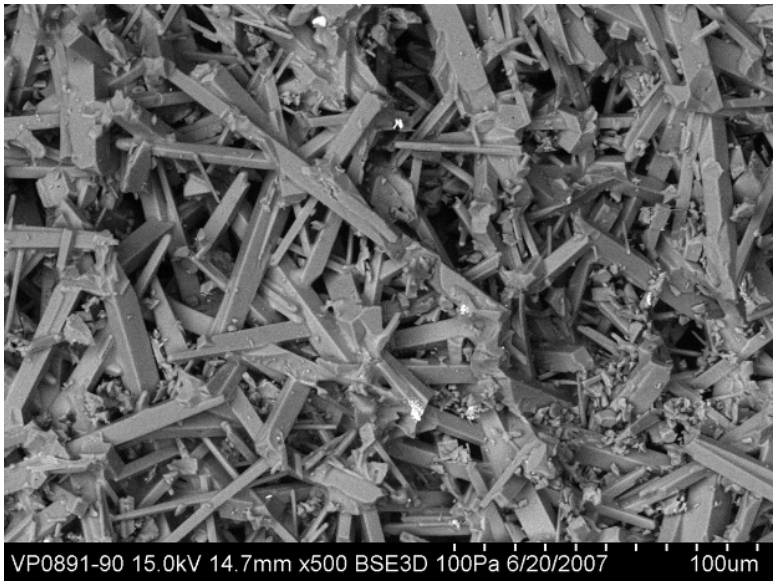

Figure 2. SEM image of the interlocking microstructure, of the mullite (D-1) DPF substrate, that is responsible for its increased fracture toughness.

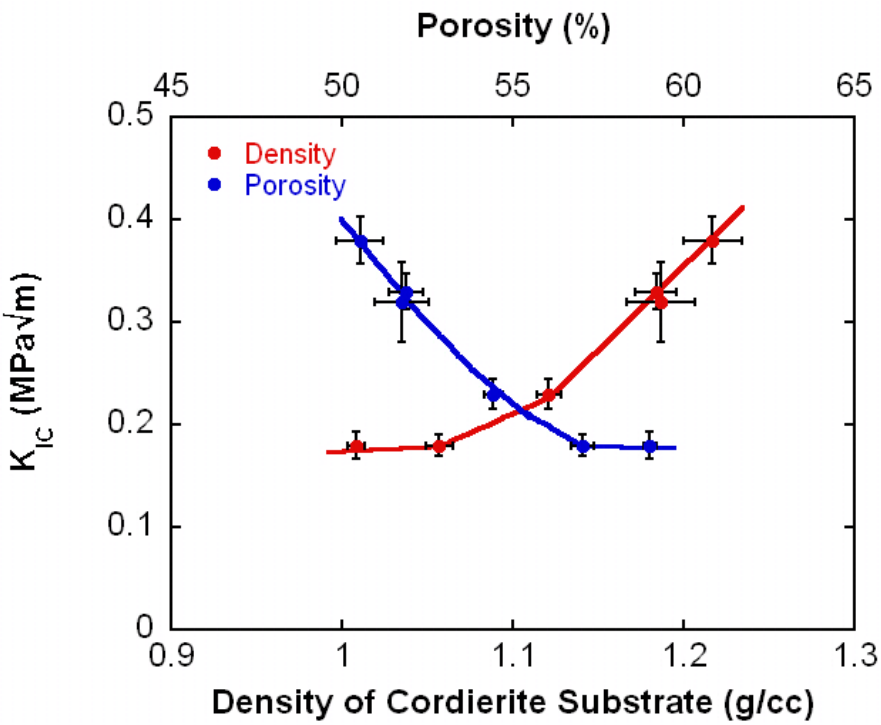

Figure 3. The variation in the fracture toughness of the cordierite substrates as a function of density and porosity of the substrate. Five specimens each were tested for C-0, C-0-Thin, C-1, B-0, B-1. Three specimens were tested for B-2 and D-1.

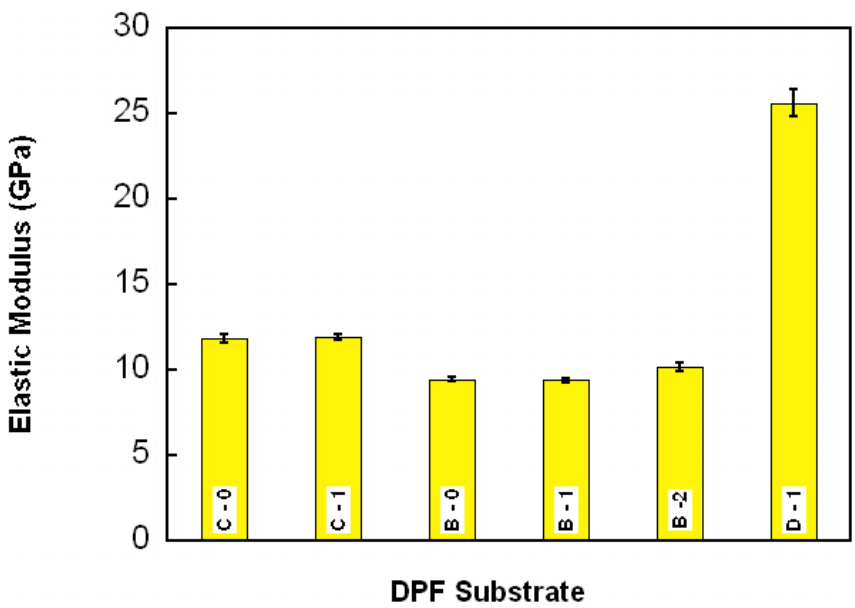

Figure 4. The room temperature elastic modulus of the DPF substrates analyzed. Isotropic elasticity was assumed. The error bars represent the RMS error of the fit for one measurement.

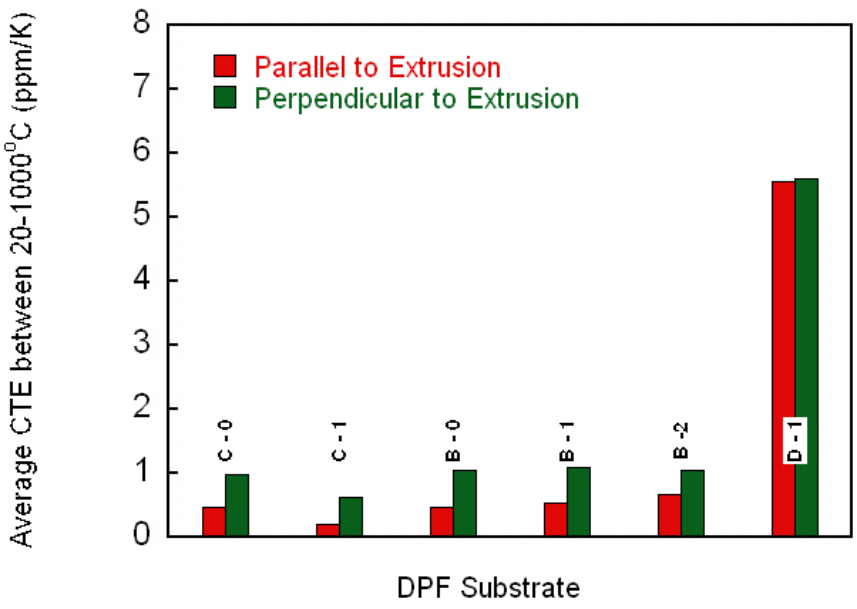

Figure 5. The coefficient of thermal expansion (CTE) of the DPF substrates analyzed. The CTE values reported are the between 20 and 1000°C and in directions that are parallel and perpendicular to the extrusion direction. One measurement each in the parallel and perpendicular direction.

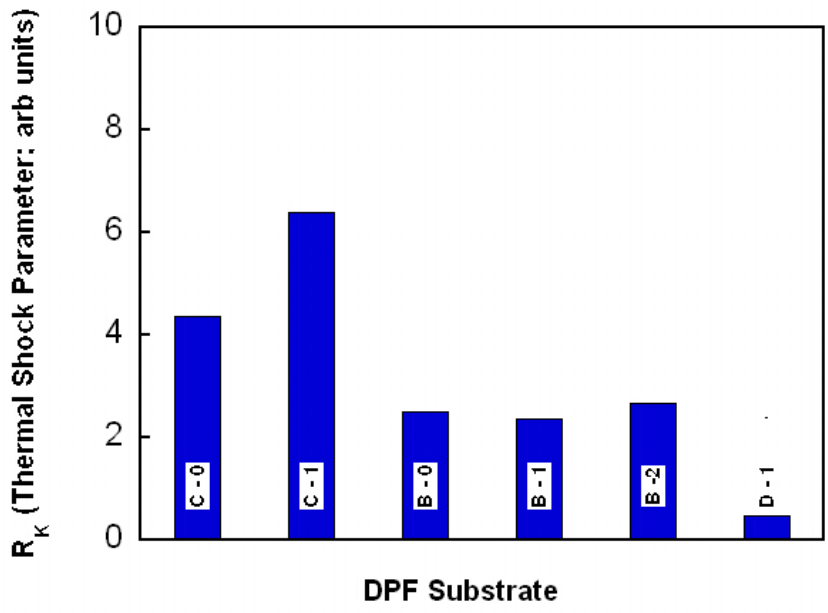

Figure 6. Comparison of the R_K, thermal shock parameter for the DPF substrates. The values are based on the average CTE (average of parallel and perpendicular values), room temperature modulus and average fracture toughness values.

Catalysis by First Principles - Can Theoretical Modeling and Experiments Play a Complimentary Role in Catalysis?

C. Narula, W. Shelton, M. Moses, L. Allard
Oak Ridge National Laboratory

Objective/Scope

This research focuses on an integrated approach between computational modeling and experimental development, design and testing of new catalyst materials, that we believe will rapidly identify the key physiochemical parameters necessary for improving the catalytic efficiency of these materials. The results will have direct impact on the optimal design, performance, and durability of supported catalysts employed in emission treatment (e.g., lean NO_x catalyst, three-way catalysts, oxidation catalysts, and lean NO_x traps etc.)

The typical solid catalyst consists of nano-particles on porous supports. The development of new catalytic materials is still dominated by trial and error methods, even though the experimental and theoretical bases for their characterization have improved dramatically in recent years. Although it has been successful, the empirical development of catalytic materials is time consuming and expensive and brings no guarantees of success. Part of the difficulty is that most catalytic materials are highly non-uniform and complex, and most characterization methods provide only average structural data. Now, with improved capabilities for synthesis of nearly uniform catalysts, which offer the prospects of high selectivity as well as susceptibility to incisive characterization combined with state-of-the science characterization methods, including those that allow imaging of individual catalytic sites, we have compelling opportunity to markedly accelerate the advancement of the science and technology of catalysis.

Computational approaches, on the other hand, have been limited to examining processes and phenomena using models that had been much simplified in comparison to real materials. This limitation was mainly a consequence of limitations in computer hardware and in the development of sophisticated algorithms that are computationally efficient. In particular, experimental catalysis has not benefited from the recent advances in high performance computing that enables more realistic simulations (empirical and first-principles) of large ensemble atoms including the local environment of a catalyst site in heterogeneous catalysis. These types of simulations, when combined with incisive microscopic and spectroscopic characterization of catalysts, can lead to a much deeper understanding of the reaction chemistry that is difficult to decipher from experimental work alone.

Thus, a protocol to systematically find the optimum catalyst can be developed that combines the power of theory and experiment for atomistic design of catalytically active sites and can translate the fundamental insights gained directly to a complete catalyst system that can be technically deployed.

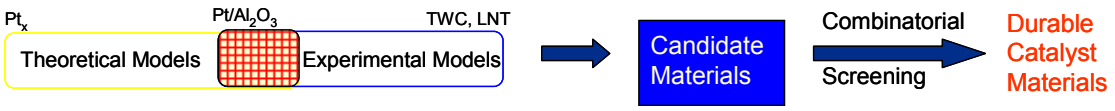

Although it is beyond doubt computationally challenging, the study of surface, nanometer-sized, metal clusters may be accomplished by merging state-of-the-art, density-functional-based, electronic-structure techniques and molecular-dynamic techniques. These techniques provide accurate energetics, force, and electronic information. Theoretical work must be based on electronic-structure methods, as opposed to more empirical-based techniques, so as to provide realistic energetics and direct electronic information.

A computationally complex system, in principle, will be a model of a simple catalyst that can be synthesized and evaluated in the laboratory. It is important to point out that such a system for experimentalist will be an idealized simple model catalyst system that will probably model a "real-world" catalyst. Thus it is conceivable that "computationally complex but experimentally simple" systems can be examined by both theoretical models and experimental work to forecast improvements in catalyst systems.

Our goals are as follows:

- Our theoretical goal is to carry out the calculation and simulation of realistic Pt nanoparticle systems (i.e., those equivalent to experiment), in particular by addressing the issues of complex cluster geometries on local bonding effects that determine reactivity. As such, we expect in combination with experiment to identify relevant clusters, and to determine the electronic properties of these clusters.
- Our experimental goal is to synthesize metal carbonyl clusters, decarbonylated metal clusters, sub-nanometer metal particles, and metallic particles (~5 nm) on alumina (commercial high surface area, sol-gel processed, and mesoporous molecular sieve), characterize them employing modern techniques including Aberration Corrected Electron Microscope (ACEM), and evaluate their CO, NO_x, and HC oxidation activity.
- This approach will allow us to identify the catalyst sites that are responsible for CO, NO_x, and HC oxidation. We will then address support-cluster interaction and design of new durable catalysts systems that can withstand the prolonged operations.

Technical Highlights

Our results on experimental studies of Platinum-Alumina Systems are summarized in the following paragraphs. The results demonstrate the impact of particle size the catalytic behavior as well as nano-structural changes in catalyst particles.

Experimental Studies:

We reported last quarter that atomic resolution imaging of 1 nm Pt/γ-Al_2O_3 by the ACEM showed the presence of single atoms and 2-3 atom clusters in addition to several 10-20 atom clusters of Pt. Our theoretical studies suggested that small atomic Pt clusters on inert supports behave similarly to free Pt clusters.

These results are in contrast to reported structure for Pt/γ-alumina. The Z-contrast imaging reports in literature describe the presence of 3-atom clusters and allocate

anomalous long Pt-Pt bonds to OH terminated Pt clusters. Recent EXAFS studies, on the other hand, suggest thermal metal-metal bond contraction after hydrogen reduction of Pt/γ-Al_2O_3 whose TEM shows particles in 0.5-1.5 nm range centered at ~0.9 nm consisting of 15±9 atoms on average.

We also reported the impact of substrate morphology by comparing the results of 2% Pt loaded on θ-Al_2O_3 with that on γ-Al_2O_3. We synthesized 12 nm Pt particles supported on γ-Al_2O_3 for this study and our results are reported.

<u>12 nm 2%Pt/ θ -Al_2O_3 Catalyst: Impact of Substrate</u>

The catalyst samples were synthesized by sintering Pt/ γ-Al_2O_3 sample at 650ºC or 5 h. The CO-oxidation tests are shown in Figure 1 and have been reported by us previously. We carried out the TEM analysis of fresh samples, sample after initiation of CO-oxidation reaction, and after 3 cycles of quantitative CO-conversion.

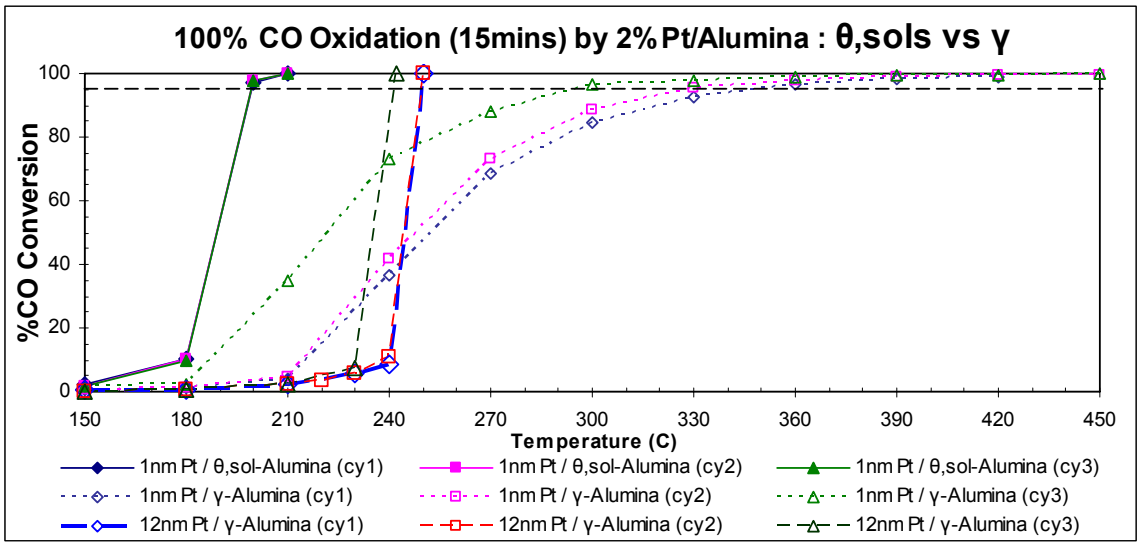

Figure 1. Quantitative CO oxidation cycled 3 times presented as a function of temperature comparing the different temperature ramps required for 1 nm Pt on θ-Al_2O_3, 1 nm Pt on γ-Al_2O_3 and 12 nm Pt on γ-Al_2O_3. The horizontal dashed line indicates 90% oxidation as the catalyst approach quantitative CO conversion

We noticed a slight particle size growth. In order to eliminate the possibility of sample-to-sample variation in particle size distribution, we carried out an *ex-situ* reactor CO oxidation aging study of this catalyst to monitor the nanostructural changes.

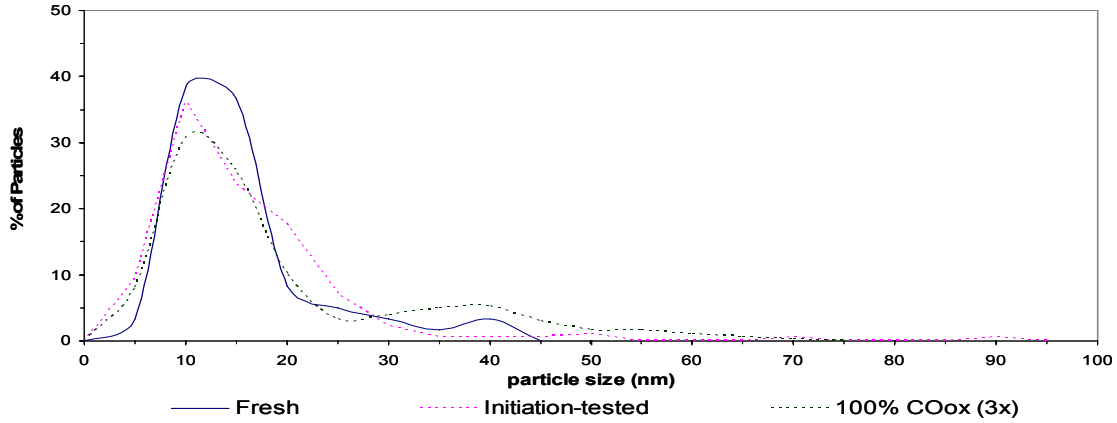

Figure 2: Changes in 12 nm 2%Pt/ γ-Al_2O_3 particle size from fresh to 3-cycles of quantitative CO oxidation based on HAADF-STEM micrographs.

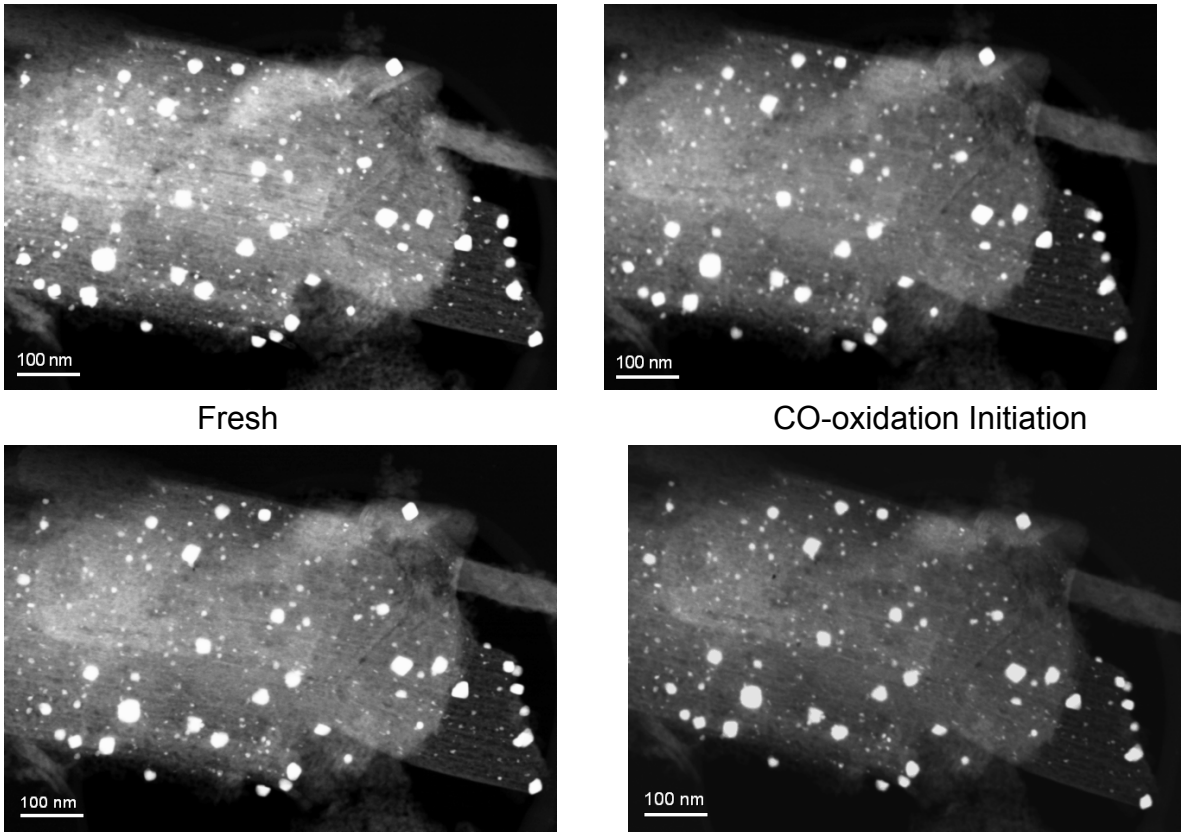

Fresh

CO-oxidation Initiation

Quantitative CO-oxidation 2 cycles cycles

Quantitative CO-oxidation 3

Figure 3: HAADF-STEM images of the exact same sample area: Fresh 2%Pt/γ-Al_2O_3 and after simulated conditions of CO oxidation Initiation and after 2-and 3-cycles of quantitative conversion.

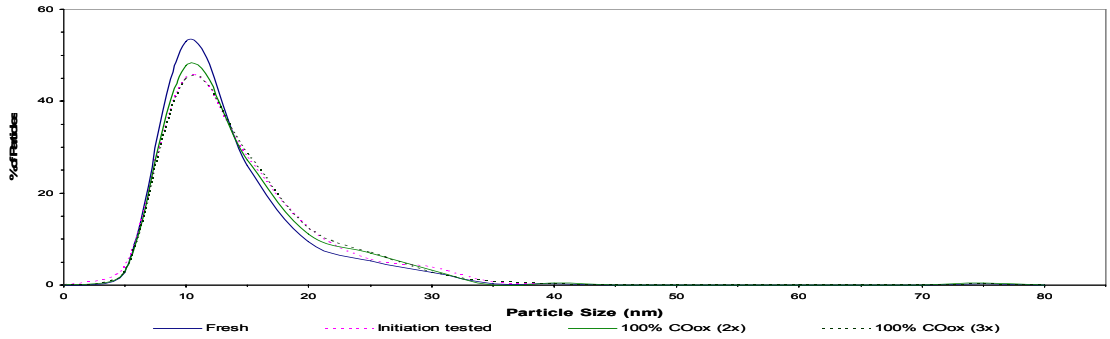

Figure 4: Pt particle size distribution in 12 nm 2%Pt/ γ-Al_2O_3 fresh catalyst and after CO oxidation on the *ex-situ* reactor, based on HAADF-STEM micrographs.

As described previously, the ex-situ reactor allows us to expose catalyst samples on a TEM grid to various catalyst operating conditions and the structural changes can then be repeatedly monitored in selected areas by electron microscopy.

Table 1. Average Pt particle size and ranges from multiple areas seen by STEM before and after CO oxidation testing.

Summary	Average	Median	Range	# of Particles
Fresh	11.1 nm	9.2 nm	2.8-39.9 nm + 72 nm	403
Initiation	11.9 nm	10.0 nm	3.0-36.7 nm + 74.3 nm	306
100% COox (2 cycles)	11.8 nm	10.0 nm	3.4-35.4 nm + 71.1 nm	243
100% COox (3rd cycle)	12.3 nm	10.4 nm	2.5-38.4 nm + 70.9 nm	238

There was practically no change in the particles (Figures 3 & 4 and Table 1) although some movement of particles was noted. This behavior of large particles is very different from nanoparticles (described previously) where 1, 2, 3, 10-20 atom clusters were observed in fresh samples that rapidly sintered under these experimental conditions. This study suggests that catalyst particles become somewhat stable as they increase in size.

The TEM analysis clearly shows that these crystalline Pt particles are not metallic on the surface and are most probably oxidized. We are analyzing the images to determine the structure of the oxide present on the surface.

Next Steps: We plan to carry out the following tasks:

- We will synthesize Pt clusters on sol-gel and molecular sieve alumina. This will create a matrix of samples with varying Pt particles size and oxidation on alumina substrates with increasing surface area and pore structure. We will carry out CO, NO_x and HC oxidation on these samples to study the effect of morphological changes in substrates leading to changes in metal substrate interactions.

- We will continue to investigate the thermal chemistry of CO and NO oxidation on free Pt and Pt oxide clusters as well as the properties of Pt and Pt oxide clusters supported on metal oxides (include magnesia and alumina). These investigations will help us gain a better understanding of the structural and catalytic properties of the supported Pt clusters and identify the effect of the support on these important properties.

Other Activities

The bench-top reactor was updated to initiate work on a joint project with John Deere Co under work for others arrangement. This update made the reactor unavailable for most of the last quarter.

Communication/Visitors/Travel

C.K. Narula presented a poster titled "Catalyst by Design - Bridging the Gap between Theory and Experiments" at DEER 2007 conference held in Detroit, MI.

Publications/Presentations

1. Narula, C. K. (speaker), Moses, M. J., Allard, L. F. "Bridging the Gap between Theory and Experiments – Nanostructural Changes in Supported Catalysts under Operating Conditions" SAE 2008 World Congress, Detroit, MI, April 2008. (Abstract Accepted).
2. Narula, C. K. (speaker), Moses, M. J., Blom, D. A., Allard, L. F. "Catalyst by Design - Bridging the Gap between Theory and Experiments", DEER 2007, Detroit, MI August, 2007.
3. Narula, C. K., Moses, M. J., Blom, D. A., Allard, L. F. "Nano-Structural Changes in Supported Pt Catalysts during CO Oxidation." North American Catalysis Society Meeting, Houston, TX, June 2007.
4. Narula, C. K., Moses, M. J., Xu, Y., Blom, D. A., Allard, L. F., Shelton, W. A. "Catalysis by Design – Theoretical and Experimental Studies of Model Catalysts." *SAE no. 2007-01-1018*, 2007.
5. Narula, C. K., Moses, M. J., Allard, L. F. "Analysis of Microstructural Changes In Lean NO_x Trap Materials Isolates Parameters Responsible for Activity Deterioration" *SAE No. 2006-01-3420*, 2006.

Ultra-High Resolution Electron Microscopy for Characterization of Catalyst Microstructures and De-activation Mechanisms

L.F. Allard, D.A. Blom, C.K. Narula, M. A. O'Keefe, M. J. Yacaman and S. A. Bradley
Oak Ridge National Laboratory

Objective/Scope

The objective of the research is to characterize the microstructures of catalyst materials of interest for the treatment of NO_x emissions in diesel and lean-burn gasoline engine exhaust systems. The research heavily utilizes new capabilities and techniques for ultra-high resolution transmission electron microscopy with the HTML's aberration-corrected electron microscope (ACEM). The research is focused on understanding the effects of reaction conditions on the changes in morphology of heavy metal species on "real" catalyst support materials (typically oxides), and the understanding of the structures of model mono-, bi- and multi-metallic catalyst systems of known particle composition. With the former systems, these changes are being studied utilizing samples treated in both steady-state bench reactors and a special *ex-situ* catalyst reactor system especially constructed to allow appropriate control of the reaction. Model samples of nanoparticulates of controlled composition on carbon or oxide supports are also being studied in collaboration with the catalysis group at the University of Texas-Austin (Prof. M. Jose-Yacaman and students). Studies of the behavior of Pt species on oxide substrates are also being conducted with colleague S. A. Bradley of UOP Co.

Technical Progress

In-Situ electron microscopy: We have begun developing a new capability to study catalyst reactions via in-situ techniques, i.e. to be able to heat and react samples inside the ACEM during imaging experiments, while retaining the capability to record images at the highest resolution levels. This effort is being done in collaboration with the company Protochips (Raleigh, NC), which provides heater elements of novel design, fabricated using semiconductor manufacturing techniques. The initial phase of the work involves testing of the heating capability alone, requiring a new specimen rod that is designed to provide electric leads in to the heating elements. There are many experiments that we are interested to conduct in which heating in vacuum (with no gas reactions) will give significant useful information. The second phase of the work will involve the development of gas reaction "cells," which will be able to be installed in a second new specimen holder that will provide gas inlet and outlet feeds. The geometry of the new technique and first imaging experiments are described below.

Protochips heater elements are fabricated from 200-micron-thick silicon chips that have a thin (20-30nm) silicon nitride film (hereafter "SiN) deposited on them. The silicon nitride film is revealed by a selective etching process, which etches the silicon and stops at the silicon nitride. The fabrication process also allows

electrical leads to be deposited (gold and copper) down onto the silicon nitride, so that when a voltage is applied, current flows through the thin film and heats it up. For the “heating-only” element, the silicon nitride film can be fabricated to have holes in it in the 3-6 micron diameter range. Figure 1a shows back-scattered electron image (BSE) from the SEM of a heater element of this geometry. Figure 1b shows the SiN film, with holes (see Fig. 3 also) drilled, and electrode area.

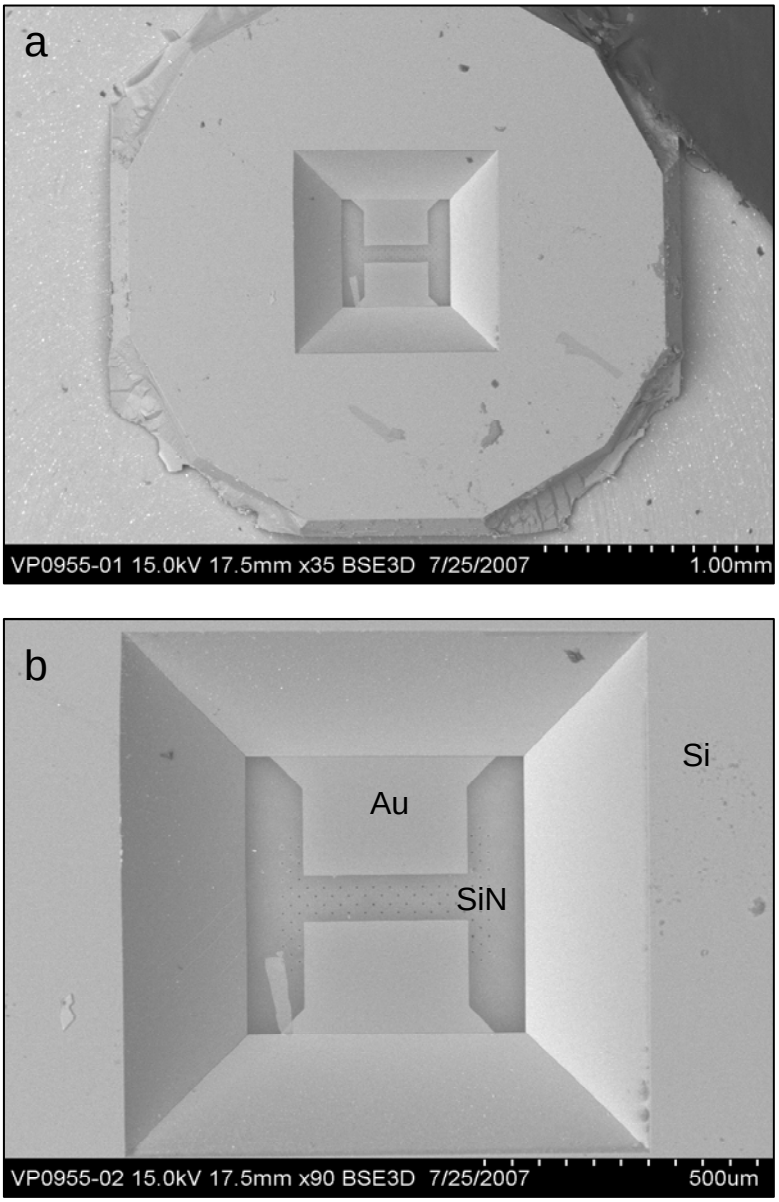

Fig. 1 a) SEM image showing entire heater chip, from the back side. b) Area of SiN heater element; the H shape is the SiN film, with gold electrodes as labeled.

A remarkable feature of the Protochips heater is that it requires very little power to raise the temperature of the silicon nitride film to very high temperatures, and the temperature increase is essentially instantaneous; for example, the temperature can be cycled from room temperature to 1100°C in 1 millisecond, and because the silicon chip support provides a large bulk of thermal sink, the film cools nearly as quickly. Bench-top experiments in a small vacuum system showed that the temperature could be calibrated with respect to the applied voltage, and that it was highly reproducible and extremely stable. With appropriate digital control of the process, we will ultimately be able to program the heating experiments to allow any heating (and reaction) sequence we require to be achieve in-situ. Figure 2 shows infrared images of the SiN film at two temperatures: ~1050°C (left) and ~1250°C (right).

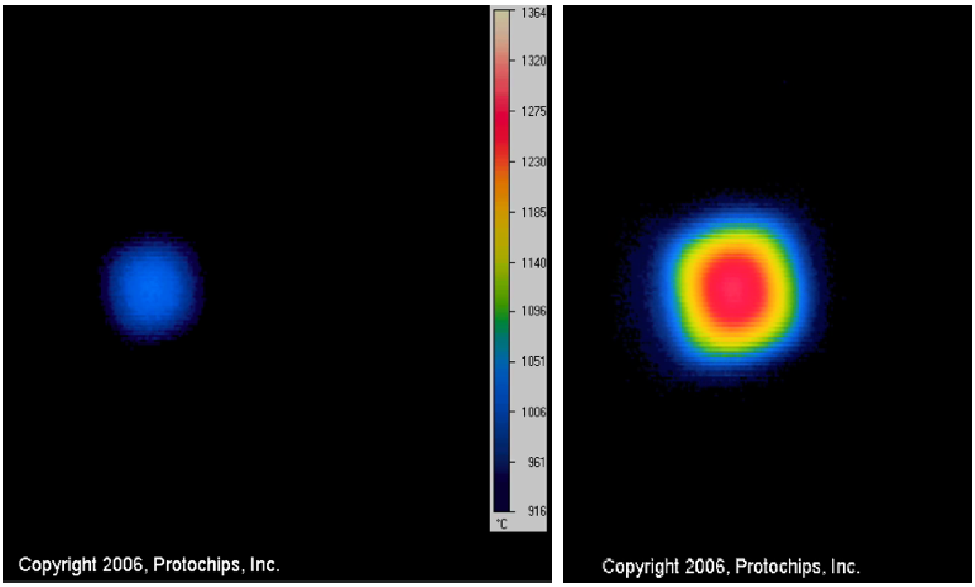

Fig. 2 Infrared images showing the SiN heater film at two different temperatures; left) about 1050°C and right) about 1250°C. Note that this experiment used a SiN film that covered the entire floor of the etched chip.

The philosophy is that the heater element can support a holey carbon film, of the type that we typically use for deposition of catalyst powders. While the silicon nitride film is itself electron transparent, and could support the powder sample directly, imaging through the silicon nitride would degrade the resolution and would not allow the full imaging capability of the ACEM to be achieved. The holey carbon film stretches over the fabricated holes in the silicon nitride, allowing the catalyst powder to be deposited either by dry-dipping the heater/film into the powder, or by depositing a droplet of powder suspended in isopropanol onto the film. Aggregates of oxide powder support material that extend over holes in the carbon are ideal areas for characterization of the catalyst structure, and ultimately the changes in morphology of particles.

We attempted to test the capabilities of the Protochips heater chip using a prototype specimen holder that had been tested in a microscope at the University of Illinois. However, the holder design did not allow it to be fit into the ultra-high-resolution objective lens pole piece on the ACEM (a new design will be tested in the next quarter). Tests of the heater on the bench, in air, allowed the demonstration of the astounding response of the SiN film to applied voltage; heating to white-hot condition was clearly essentially instantaneous.

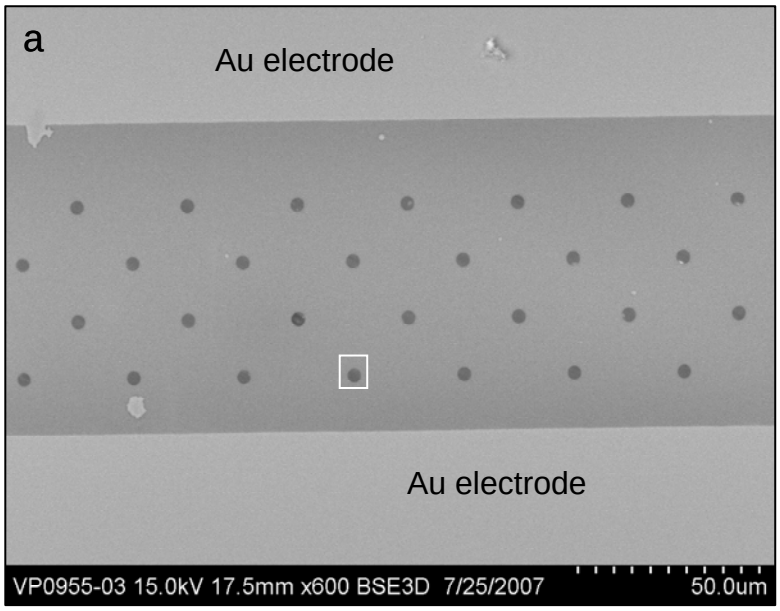

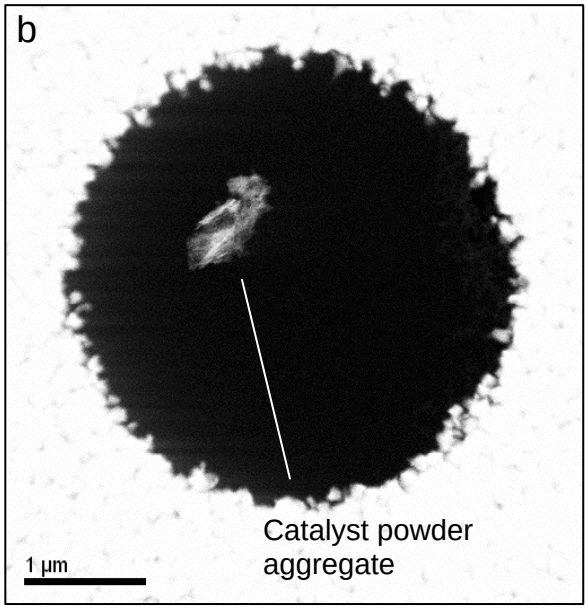

Fig. 3 a) Patterned 3-micron diameter holes in the SiN thin film heater element. Gold electrodes are labeled. b) dark-field image from the ACEM showing a single hole with holey carbon film and a Pt/Al_2O_3 powder aggregate on the film.

There remained the question of whether the heater chip would allow imaging of single atomic species on real catalyst supports. This was tested by installing the chip into the standard double-tilt JEOL specimen holder, and examining the deposited catalyst material (Pt on Al_2O_3) in the ACEM. Figure 3a shows the silicon nitride film at higher magnification, and Fig. 3b is a single hole with an aggregate of powder visible on the holey carbon support.

Figures 4a and 4b show increasing magnifications, with the image of Fig. 4b showing single atoms and very small clusters clearly imaged. Thus there is strong promise that the Protochips heaters, when installed in an appropriate specimen rod, will allow us to conduct imaging experiments on our catalyst samples in-situ, and thereby have a new tool in our studies of the effects of processing on catalyst degradation. The first tests of the in-situ heating capability will be reported in the next quarterly.

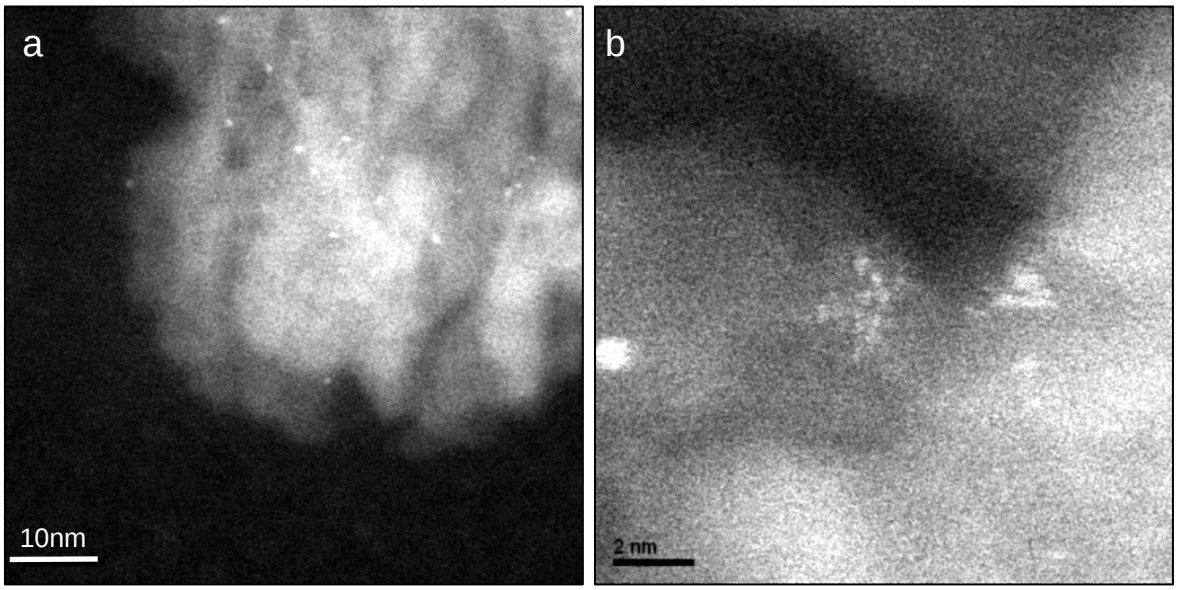

Fig. 4 a) Dark-field image of a powder aggregate, showing 0.5-1nm Pt clusters; b) higher magnification dark-field image showing a discrete 1nm cluster of Pt atoms at the left side, and a loose 'raft' of individual atoms in the center. This illustrates the ability to do atomic level imaging using the Protochips heater chip.

References

1. US Patent Application Publication No. 2006/0025002 A1

Status of Milestones

On schedule

Communications/Visits/Travel

None this period

Publications

None this period

Life Prediction of Diesel Engine Components

H. T. Lin, T. P. Kirkland, and A. A. Wereszczak
Oak Ridge National Laboratory

Nate Phillips and Nan Yang
Caterpillar

Objective/Scope

The valid prediction of mechanical reliability and service life is a prerequisite for the successful implementation of structural ceramics and advanced intermetallic alloys as internal combustion engine components. There are three primary goals of this research project which contribute toward that implementation: the generation of mechanical engineering data from ambient to high temperatures of candidate structural ceramics and intermetallic alloys; the microstructural characterization of failure phenomena in these ceramics and alloys and components fabricated from them; and the application and verification of probabilistic life prediction methods using diesel engine components as test cases. For all three stages, results are provided to both the material suppliers and component end-users.

The systematic study of candidate structural ceramics (primarily silicon nitride) for internal combustion engine components is undertaken as a function of temperature (<1200°C), environment, time, and machining conditions. Properties such as strength and fatigue will be characterized via flexure and rotary bend testing.

The second goal of the program is to characterize the evolution and role of damage mechanisms, and changes in microstructure linked to the ceramic's mechanical performance, at representative engine component service conditions. These will be examined using several analytical techniques including optical and scanning electron microscopy. Specifically, several microstructural aspects of failure will be characterized:

(1) strength-limiting flaw-type identification;
(2) edge, surface, and volume effects on strength and fatigue size-scaling
(3) changes in failure mechanism as a function of temperature;
(4) the nature of slow crack growth; and
(5) what role residual stresses may have in these processes.

Lastly, numerical probabilistic models (i.e., life prediction codes) will be used in conjunction with the generated strength and fatigue data to predict the failure probability and reliability of complex-shaped components subjected to mechanical loading, such as a silicon nitride diesel engine valve. The predicted results will then be compared to actual component performance measured experimentally or from field service data. As a consequence of these efforts, the data generated in this program will not only provide a critically needed base for component utilization in internal combustion engines, but will also facilitate the maturation of candidate ceramic materials and a design algorithm for ceramic components subjected to mechanical loading in general.

Technical Highlights

Silicon nitride and TiAl exhaust valves

Detailed SEM studies of stem surface and fracture surfaces of selected half cylindrical stem specimens were carried out to identify the key strength limiting flaws during this reporting period. Figure 1 compares the SEM stem surface features between as-received and 500-h-tested valve stem. Many of the original machined groves disappeared due to the repeatedly reciprocating frictional movement between the valve guide and stem (Fig. 1b), resulting in a much smoother surface, consistent with the measured higher retained fracture strength reported previously. In regions in close contact with valve guide the surfaces are so smooth similar to the etched surfaces (Fig.1c). Figure 2 shows the SEM fracture surface of as-received and 500-h-tested valve stems. In general, all of the as-received specimens failed from the original machined flaw, critical grove ~ 150-200 µm in length (Fig.2a). As for the 500-h-tested specimens there are also many failing from the remnant machining flaws (Fig. 2b), while few failed from the processing flaw, i.e., pores (Fig. 2c). On the other hand, selected 500-h-tested valve heads of both silicon nitride and TiAl were mechanically tested to evaluate the effect of engine environment on the retained strength. These valve heads were tested in compression via a special custom designed test fixture to generate the highest principal tensile stress in the vale head-stem transition region. Note that as-received valve heads were also tested for comparison. Figure 3 shows the fracture strengths for the 500-h-tested and as-received silicon nitride and TiAl valve heads. Due to the very limited number of valve heads tested the mechanical results would not provide any statistical insight. However, results suggested that the engine environment cause no or little mechanical degradation of both silicon nitride and TiAl valves after 500-h field test. Detailed optical fractography and SEM analysis will be carried out on selected fracture valve heads to elucidate the cause of fracture. Note that the setup of the second 500-h engine test was completed and test has been initiated in order to achieve a total of 1000-h engine test times on both silicon nitride and TiAl valves.

High-temperature Creep of TiAl intermetallic alloys

Studies of long-term creep behavior in air of TiAl alloys manufactured by Daido and Howmet were continued during this reporting period, and were mostly focusing on Daido Non-HIP, designated as RNT650, and Howmet TiAl, designated as 45XD. The test conditions specified are relevant to the temperature and tensile stress profiles imposed on the TiAl turbo wheel under the engine operational conditions obtained via the FEA modeling task carried out by end users. The database generated from these long-term tensile creep studies will then be used for verification of probabilistic component design and life prediction task critical to end users. Also, these data could provide important feedbacks to material suppliers for process refinements to further improve the alloy mechanical reliability and performances, especially the high-temperature fatigue and creep properties. Figure 4 compares the effect of sintering process on the creep behavior of Daido TiAl alloy. Note that the creep data of HIP TiAl have been reported previously. Tensile creep results of Daido TiAl alloys indicated that there might be an effect of densification method (HIP vs. non-HIP) on the creep deformation rate under the similar test conditions employed, which might result from the

difference in microstructure; i.e., colony grain size and lamellar thickness. More tests need to be carried out to obtain a better statistical trend of microstructure effect. On the other hand, the preliminary creep rate versus applied stress curves showed that the Daido HIP TiAl exhibited creep resistance than Howmet 45XD Fig. 5, which is more apparent at the higher temperature and stress regime. Creep tests at lower stress levels as a function of test temperature are in progress to elucidate the creep controlling mechanisms and thus life limiting processes for both alloys.

Status of Milestones

Milestone: "Complete mechanical testing and analysis of prototype silicon nitride and TiAl valves after natural gas engine field test." On schedule.

Communications / Visitors / Travel

Communication with Nate Phillips at Caterpillar, and Norberto Domingo and Michael Kass at NTRC on the updates of microstructure characterization and mechanical testing of 500-h-tested Si_3N_4 and TiAl valve stems and heads.

Communication with Nate Phillips at Caterpillar on the specimen preparation status and test matrix for the Ceradyne SN147 silicon nitride cylindrical rods after machined via various machining parameters.

Communications with Nan Yang at Caterpillar on the update of tensile creep tests for both Daido and Howmet TiAl materials.

Problems Encountered

None

Publications

None

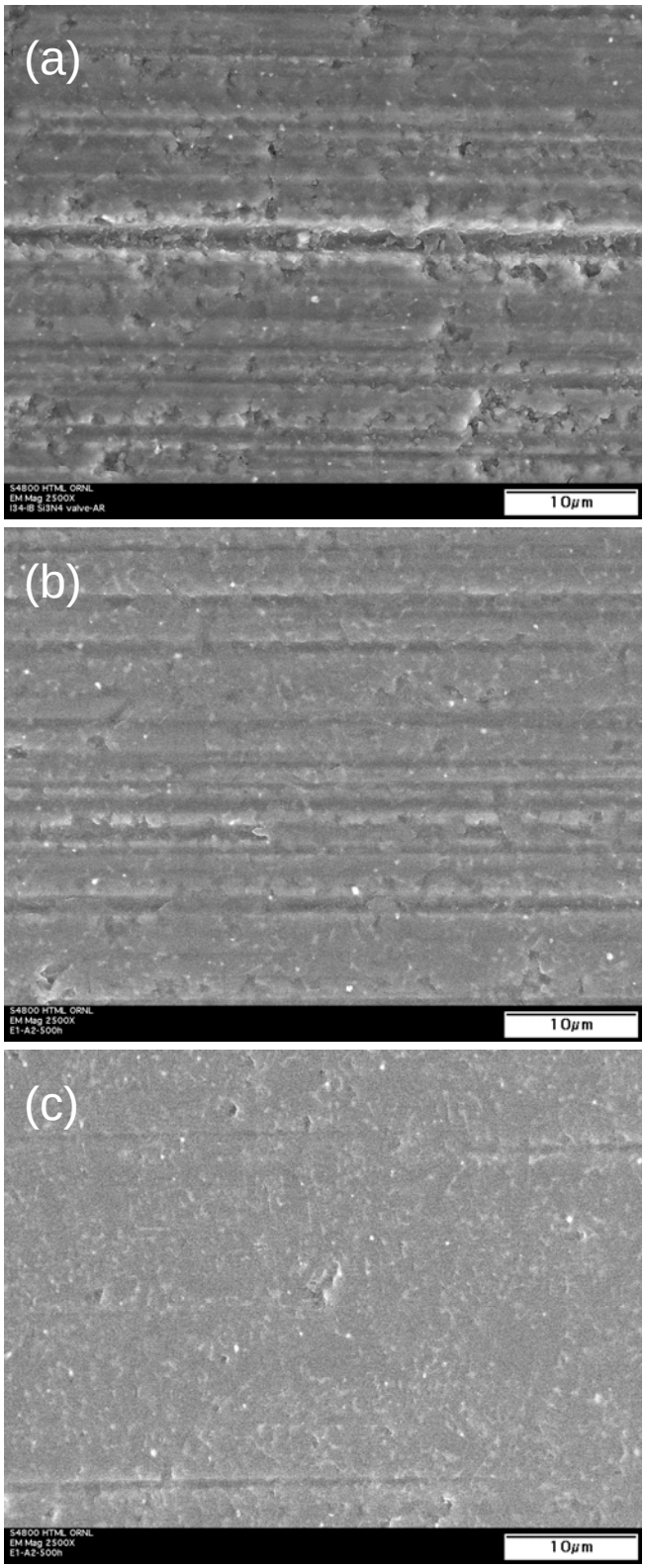

Figure 1. SEM surface features of silicon nitride half cylindrical stems before (a) and after 500-h engine test (b & c).

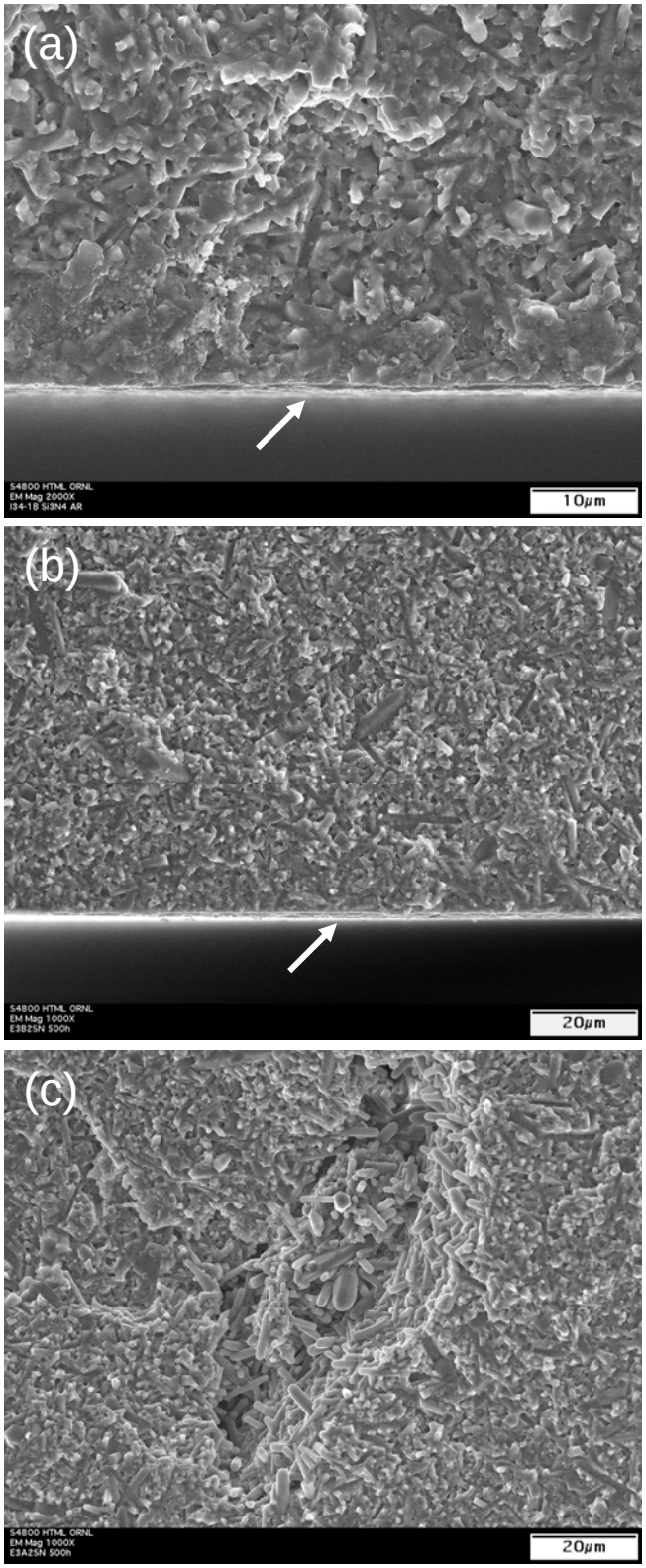

Figure 2. SEM fracture surfaces of half cylindrical SN235P silicon nitride exhaust valves after 500-h test (a) and in as-received condition (b & c).

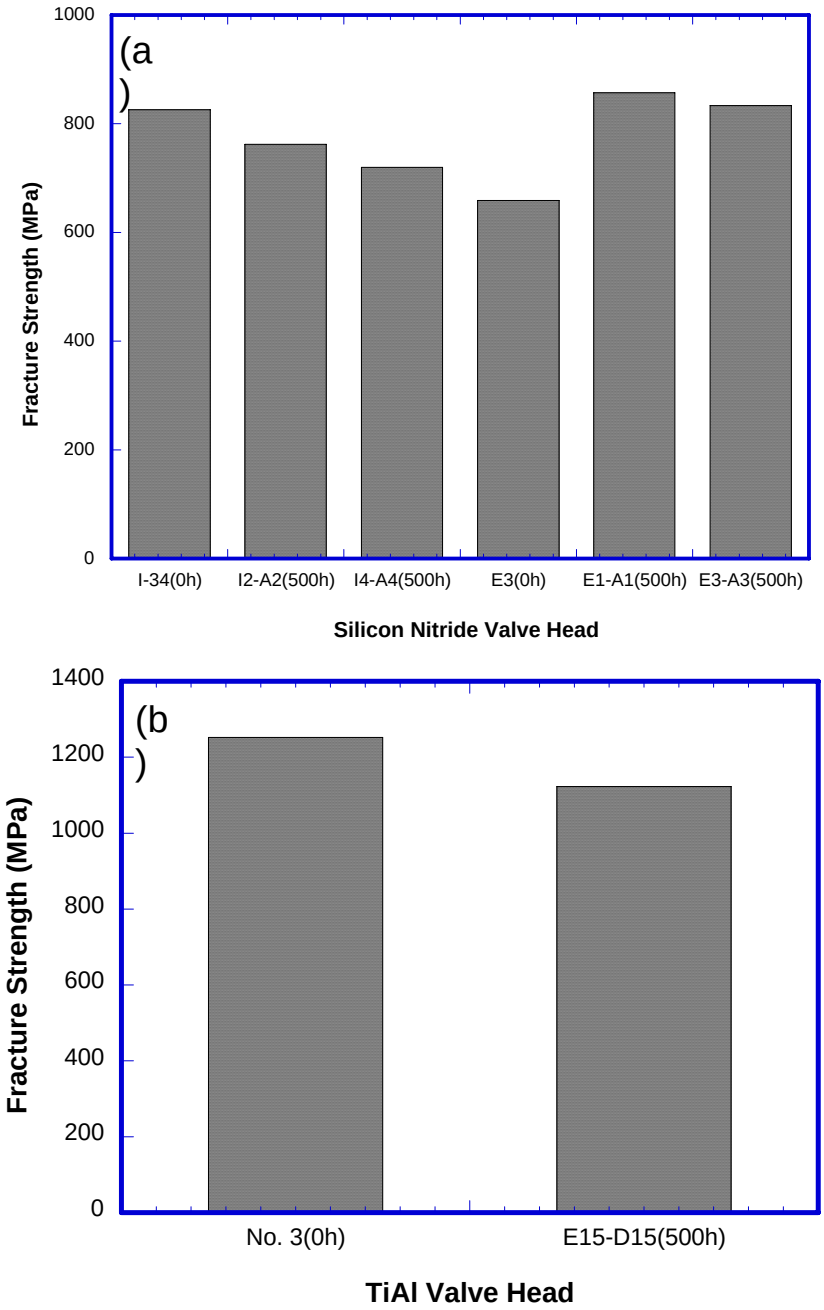

Figure 3. Fracture strength comparison between as-received and 500-h test valve head of (a) silicon nitride valves and (b) TiAl valves.

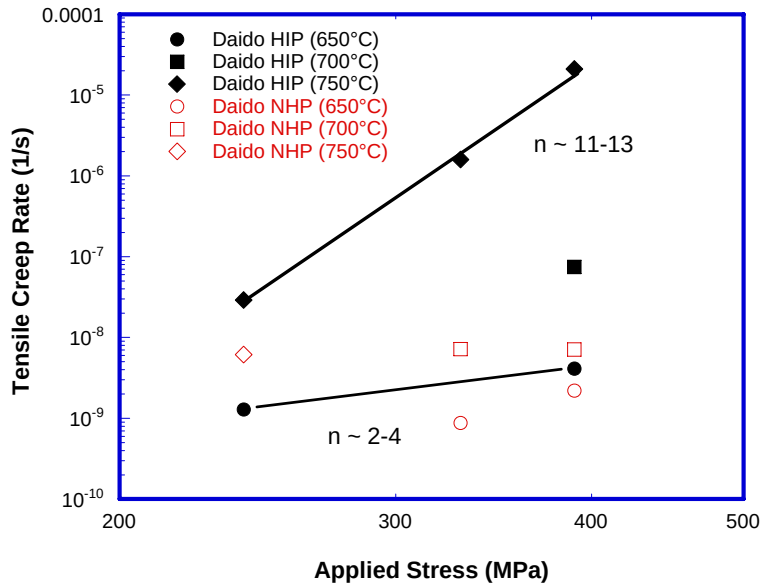

Figure 4. Creep rate versus applied stress curves of Daido TiAl alloy.

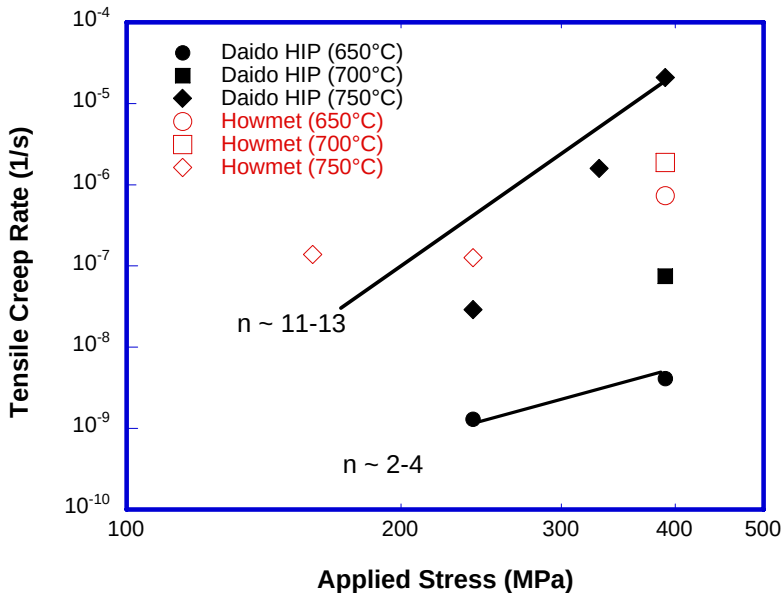

Figure 5. Creep rate versus applied stress curves of Daido HIP and Howmet TiAl alloy.

Powder Processing of Nanostructured Alloys Produced by Machining

S. Chandrasekar, K. P. Trumble, and W. D. Compton
Purdue University

Objective/Scope

Work has continued on production of bulk ultrafine-grained (UFG) alloys by machining and consolidation of UFG particulate created by machining. Additionally, scale-up of a method for production of nanostructured particulate by machining has been initiated.

Technical Highlights

Large strain extrusion machining is being implemented in a linear machining configuration on a press. The use of a press will enable plate samples of a large size to be created. Initial work is focusing on Al 6061T6, CP-titanium and copper as model materials to demonstrate production of plates with sizes on the order of 25x25x3mm. Where necessary, heating of the tool and deformation zone can be implemented to facilitate the extrusion machining.

Methods to scale-up production of particulate by modulation-assisted machining are also in progress. Successful scale-up will ensure a cost-effective method for manufacture of particulate with ultrafine grained microstructure. This method is likely to offer important benefits for production of particulate in materials systems such as those of Ti, Al and Mg.

Other Highlights

James Mann, a PhD student working on this program, established a start-up company, M4 Sciences, in 2006 to commercialize technologies in modulation-assisted machining and nanostructured particulate materials. This company won the Burton Morgan Business plan competition, considered the premier competition of its kind in the state of Indiana, in March 2007. M4 Sciences is also a recipient of an NSF STTR award.

Chris Saldana, a PhD student working on this program, presented papers at the Indiana Advancing Manufacturing Summit in May 2007 and at the Severe Plastic Deformation 2007 meeting in Ufa, Russia, in August 2007. The former won first place out of ~ 50 posters and the latter won a bronze medal award in the young scientist category. The Indiana Advancing Manufacturing Summit was attended by ~ 400 people from industry, Federal and State governments and National Labs.

Problems Encountered

None

Status of Milestones

"Evaluate a range of consolidation and densification routes that enable bulk monolithic and composite materials to be produced from nanostructured machining chip particulate without significant coarsening." On schedule.

Publications

J. B. Mann, C. Saldana, S. Chandrasekar, W. D. Compton and K. P. Trumble, Metal particulate production by modulation-assisted machining, *Scripta Materialia* **57**, 909-912, 2007.

Modeling of Thermoelectrics

A. A. Wereszczak and O. M. Jadaan
Oak Ridge National Laboratory

Objective/Scope

Potential next generation thermoelectric (TE) devices comprised of p- and n-type oxide ceramics enjoy strong interest for implementation in high temperature and oxidizing environments because their waste heat could be used to generate electricity. However, the intended TE function of these devices will only be enabled if the device is designed to overcome the thermomechanical limitations (i.e., brittleness) inherent to these oxides. A TE oxide with a combination of poor strength and low thermal conductivity can readily fail in the presence of a thermal gradient thereby preventing the exploitation of the desired thermoelectrical function.

This seemingly insurmountable problem can be overcome with the combined use of established probabilistic design methods developed for brittle structural components, good thermoelastic and thermomechanical databases of the candidate oxide material comprising the TE device, and iteratively applied design sensitivity analysis. This project executes this process by interrogating the reliability of prototypical TE devices (e.g., thin-film-based) and oxides.

There will be several outcomes from this work that will benefit TE oxide and device developers and end-users of these potentially high temperature TE devices: mechanical reliability of prototypical TE devices will be evaluated from a structural ceramic perspective and suggested redesigns will be identified, thermomechanical reliability of developmental TE oxides will be assessed, and minimum required thermomechanical properties of hypothetical TE oxides would be identified that produce desired reliability in a TE device. Additionally, innovative and cost-effective methods to process high temperature capable TEs will be a part of this project's research portfolio.

Technical Highlights

Finite element analysis (FEA) stress analysis for an arbitrary thermoelectric (TE) module was performed. Subsequent probabilistic design sensitivity (PDS) analysis will be conducted in the fourth quarter to determine which parameters have the largest effect on first principal tensile stress in the TE legs and alumina substrates.

Figure 1 shows the geometry of the TE module with colors corresponding to material sequence. In this schematic, purple corresponds to the alumina insulator plates, turquoise is steel contacts, while red is the TE legs. Figure 2 shows various views of the TE module with the insulator plates removed in order to clearly display the geometric arrangement of the steel contacts.

Thermal Solid90 and structural solid95 elements in ANSYS were used to simulate the device and conduct the thermomechanical stress analysis. Figure 3 shows the mesh distribution used in the simulation which contained 142899 elements and 240989 nodes.

Figure 4 shows the temperature distribution throughout the TE device. In this steady state thermal analysis, the temperatures were set to 533 ºC at the top surface of the hot alumina plate and 78 ºC at the bottom surface of the cold alumina plate.

Figure 5 displays the first principal stress distribution in the entire TE device due to the 455 ºC temperature gradient shown in Fig. 5. A maximum stress of 1105 MPa develops in the module and is located within the stainless steel contacts as can be seen from Fig. 6.

This work was mainly concerned with the reliability of the brittle materials from which the TE legs as well as the alumina plates are made. Figure 7 demonstrates that the maximum tensile stress in the TE material reaches 382 MPa in localized areas, while in the alumina plates (Fig. 8) the stress goes up to 815 MPa. Given that the strength of the thermoelectric material is estimated to be ~100 MPa, while that for alumina is 400-550 MPa, it can be seen that this design will not survive the intended service load per Fig. 5.

These results provide the necessary background to initiate PDS analysis which will be conducted in the fourth quarter.

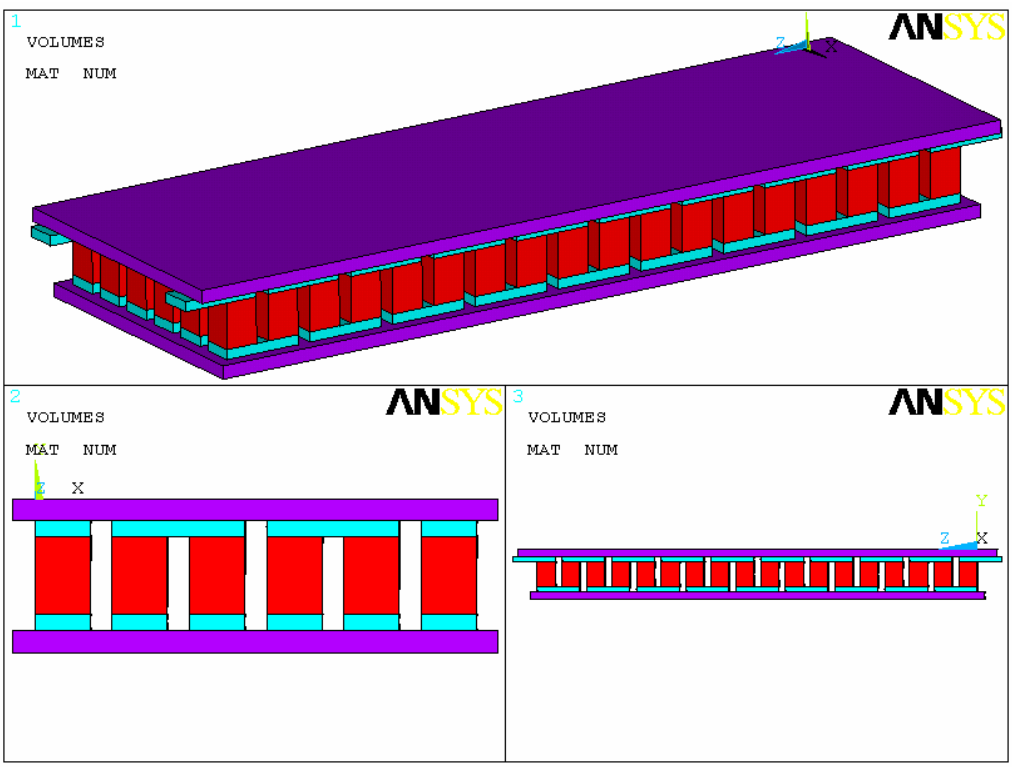

Figure 1. Various views of the TE module with colors corresponding to material sequence. Purple is the alumina insulator plates, turquoise is the steel contacts, while red is the TE legs.

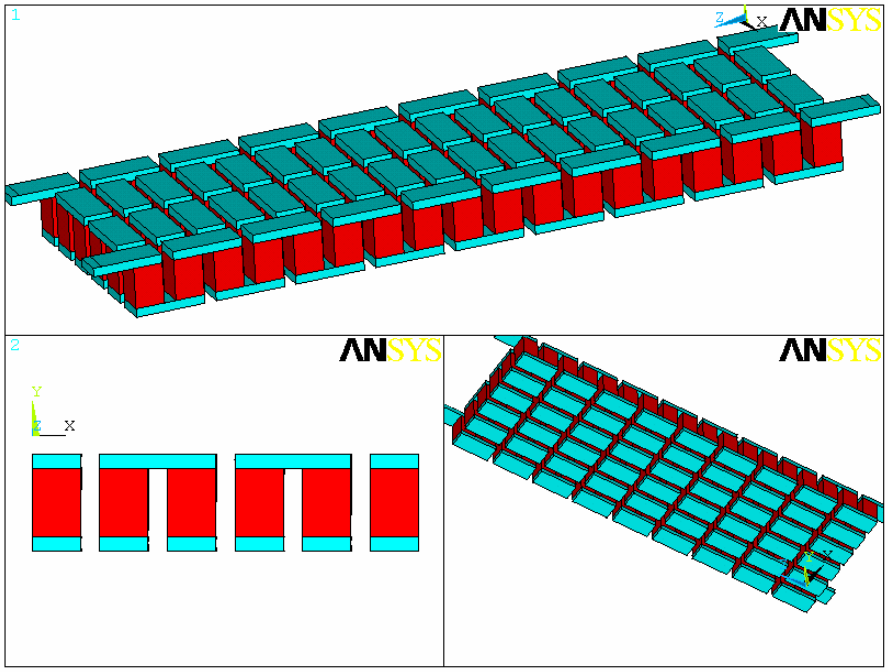

Figure 2. Various views of the TE module with the insulator plates removed in order to display the geometric arrangement of the steel contacts.

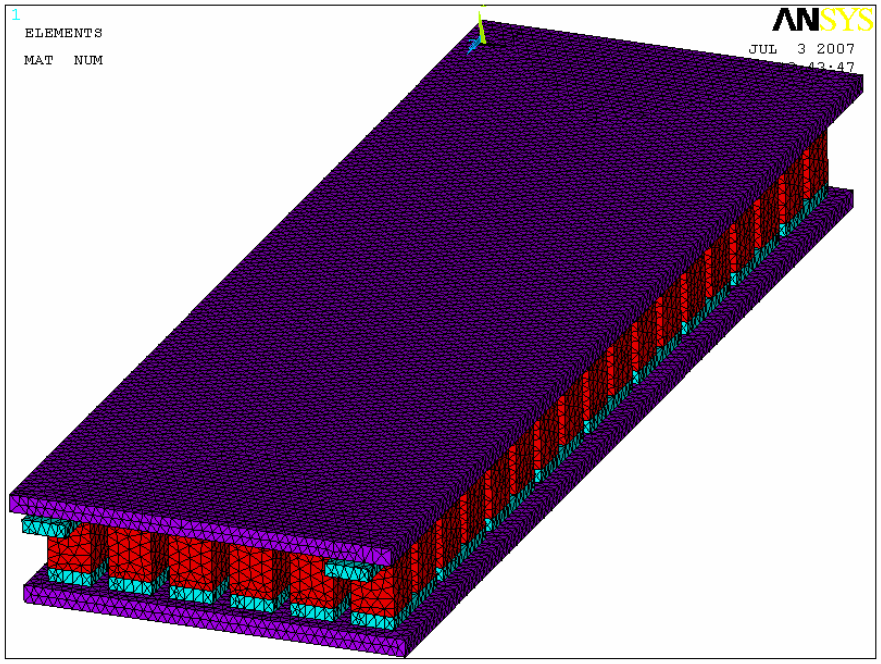

Figure 3. Mesh distribution showing solid 95 elements. The mesh contains 142899 elements and 240989 nodes.

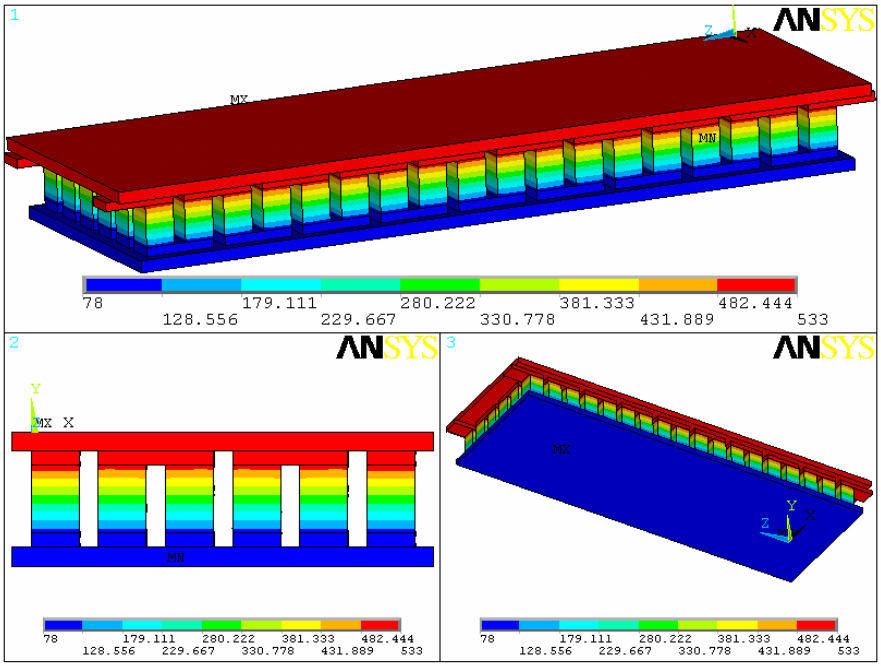

Figure 4. Temperature distribution in the TE module in degrees Celsius.

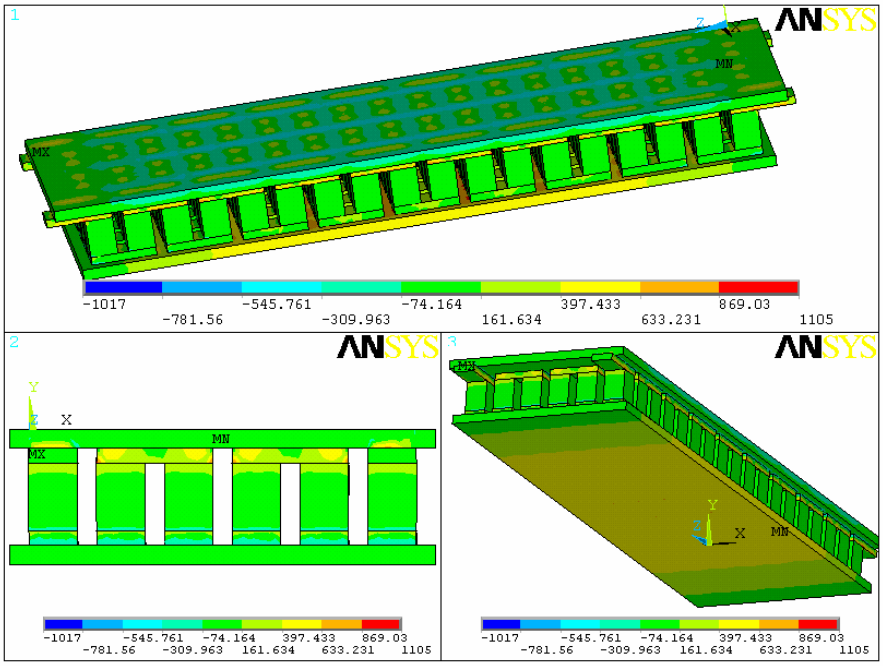

Figure 5. First principal stress distribution in the TE device due to the thermal loading shown in Fig. 4.

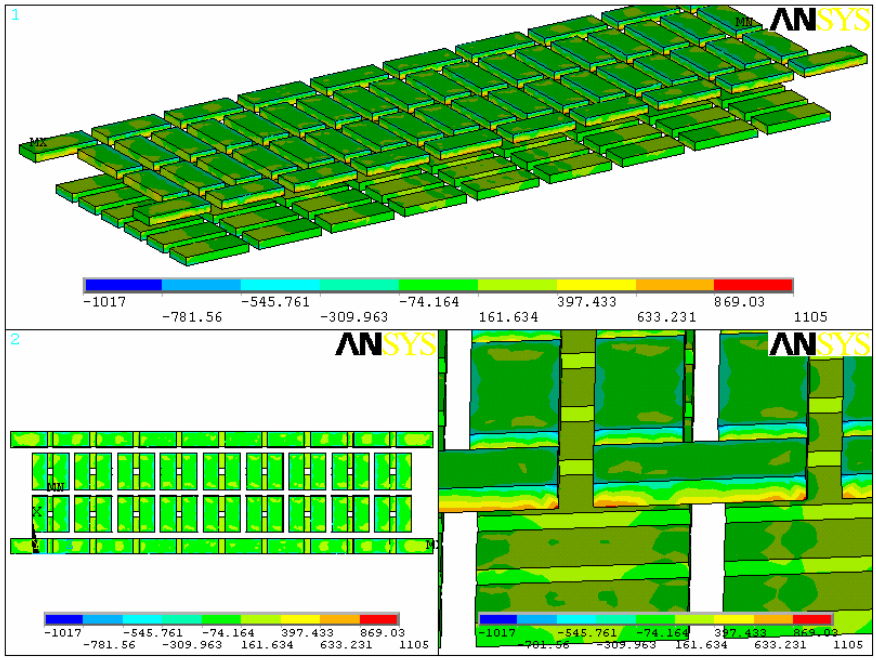

Figure 6. First principal stress distribution in the stainless steel contacts due to the thermal loading shown in Fig. 4.

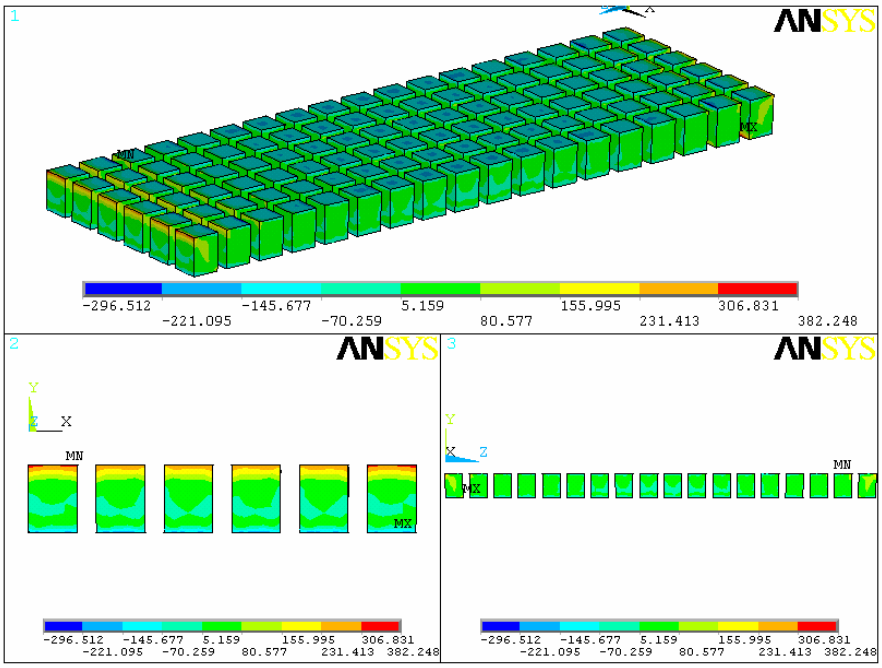

Figure 7. First principal stress distribution in the TE legs due to the thermal loading shown in Fig. 4.

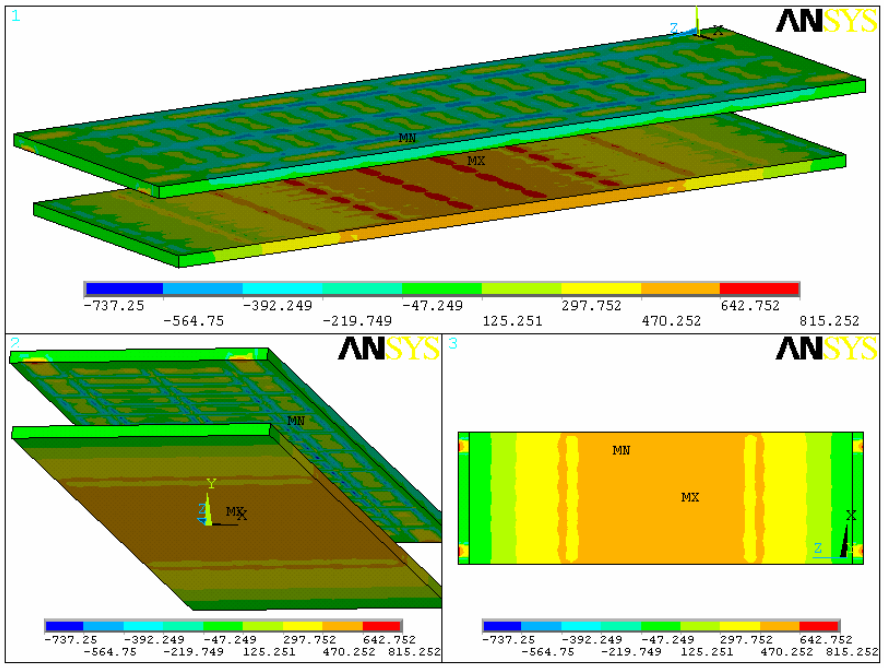

Figure 8. First principal stress distribution in the alumina insulation plates due to the thermal loading shown in Fig. 4.

Status of FY 2007 Milestones

Perform probability design sensitivity analysis on a TE device and rank those material properties or dimensions whose control would have the largest effect on reliability. **(Sep07)** *On schedule.*

Communications/Visits/Travel

Wereszczak participated in a conference call on June 28 with staff from General Motors, General Electric, the University of South Florida, Michigan St. University, and the University of Michigan. Wereszczak also had several communications with Jihui Yang of General Motors and Todd Anderson of General Electric about thermoelectric material properties.

Publications

An abstract entitled “Probabilistic Design Optimization and Reliability Assessment of High Temperature Thermoelectric Devices” by O. Jadaan and A. A. Wereszczak was submitted to the 2008 ICACC to be held in Daytona Beach in January 2008.

References

None.